Chapter 29

Ocean Heat Transport

Alison M. Macdonald* and Molly O. Baringer†

*Woods Hole Oceanographic Institution, Woods Hole, Massachusetts, USA

†NOAA/Atlantic Oceanographic and Meteorological Laboratory, Miami, Florida, USA

Chapter Outline

1. BACKGROUND

At the top of the atmosphere, the global energy balance is solely determined as the difference between the amount of solar energy that is absorbed by the earth and the amount reflected and reemitted back into space. At the surface, however, it is the distribution of the incoming and outgoing components that determines the balance and defines the climate of the environments in which we live. Radiant solar energy drives movement within the atmosphere and ocean, and the resulting circulation patterns within both systems provide feedbacks that continuously define and shape the global energy budget. This intertwined relationship between the atmosphere and ocean implies that oceanic transports of mass, and heat in particular, but more generally all properties, are intrinsically related to one another. They are affected by, and in some cases can affect, atmospheric circulation and conditions. Although both the atmosphere and ocean behave according to the laws of thermal and fluid dynamics, their differences allow them to play contrasting roles in the global energy balance. The ocean has a much greater capacity for energy storage and, being comparatively slow, has a long thermal memory. The atmosphere, moving more quickly, is an efficient mixer. Understanding the flow of energy both within and between the two systems is fundamental to our understanding and prediction of both natural climate variability and anthropogenically induced climate change.

In this chapter, as well as elsewhere in the literature, ocean heat transport is discussed with the recognition that although temperature is a property of water, heat is not. Here, the term *heat transport* is used synonymously with the more correct term *energy transport* (see Bryan (1962) and Warren (1999) for more complete discussions), while we reserve the term *temperature transport* for enthalpy, that is, for the specific instance where mass is not balanced (see Section 2.2). Several acronyms are used throughout the text. OHT refers to ocean heat transport. The term MHT refers specifically to meridional heat transport and is used here only in reference to the ocean. MOC is meridional overturning circulation.

In this chapter, we provide some historical background on the various methods used to calculate OHT and the resulting estimates; discussion of the techniques that have been used to decompose these estimates so as to better understand the physical mechanisms involved; and a discussion of OHT variability and its effects on OHT estimates. The reader is referred to earlier chapters such as 7

Ocean Circulation and Climate, Vol. 103. http://dx.doi.org/10.1016/B978-0-12-391851-2.00029-5

and 8 (diapycnal and lateral transport, respectively), 9 and 10 (overturning circulation), 11 (wind-driven circulation), and 13 and 14 (western and eastern boundary currents, respectively) for more in-depth consideration of the underlying circulation.

1.1. Energy Balance in the Atmosphere

At the top of the atmosphere, the global energy balance is between total incoming radiation from the sun and total outgoing radiation. The latter includes reflected solar radiation and emitted blackbody radiation. Total solar irradiance at the top of the atmosphere, also known as the solar constant (S), has a canonical mean value of 1365.4 ± 0.7 Wm^{-2} (Lee et al., 1995) and varies with the 11-year sunspot cycle by 1–2 Wm^{-2} (Lee et al., 1995; Willson and Hudson, 1991). The total solar radiation that the earth receives at the top of the atmosphere is a function of the earth's cross-section (πr^2) and because it rotates, its surface area ($4\pi r^2$). Therefore, the net incoming solar radiation is one-fourth the solar constant, $S/4$.

Estimates of the earth's radiation budget were made as early as 1837, but it was not until the early 1900s that a ground-based monitoring observatory allowed for observed estimates of incoming shortwave and outgoing longwave radiative components to be made (Abbot and Fowle, 1908 from Hunt et al., 1986). A balance was obtained using a global annual average incident solar flux of 364.4 Wm^{-2} based on the local observatory measurements. A decade later, Dines (1917) (from Hunt et al., 1986) improved upon this calculation, including terms representing downward longwave radiation from the atmosphere and upward nonradiative fluxes from the surface. These early estimates were not unreasonable, but they contained much detail based on broad assumptions made necessary by the dearth of observations. By the 1950s, ground-based observations had developed to the point that truly global estimates were possible. Hunt et al. (1986) attribute the first global study to London (1957).

The first satellite capable of observing meteorology was launched in 1959, but it was the Nimbus satellite program of the 1970s that flew instruments specifically designed to observe the earth's net energy budget at the top of the atmosphere by directly measuring solar irradiance, reflected shortwave radiation and emitted longwave radiation. It provided the first global continuous time series of these radiative components (House et al., 1986). Today's estimates of these components of the global energy budget (Figure 29.1) have been further refined by satellite monitoring of the top of the atmosphere, as well as by radiative models that estimate the partitioning of energy for different atmospheric conditions (e.g., high clouds, cloud-free, etc.). Together, these estimates suggest that about 23% of incoming solar radiation is reflected back out into space by the atmosphere. The atmosphere itself absorbs approximately the same amount, and yet it emits a great deal more (~60% of the incoming value) due to the complex energy exchange between the atmosphere and the surface of the earth. The earth as a whole, including the ocean, absorbs approximately half the incoming solar radiation (Figure 29.1), which is then returned to the atmosphere through remitted blackbody

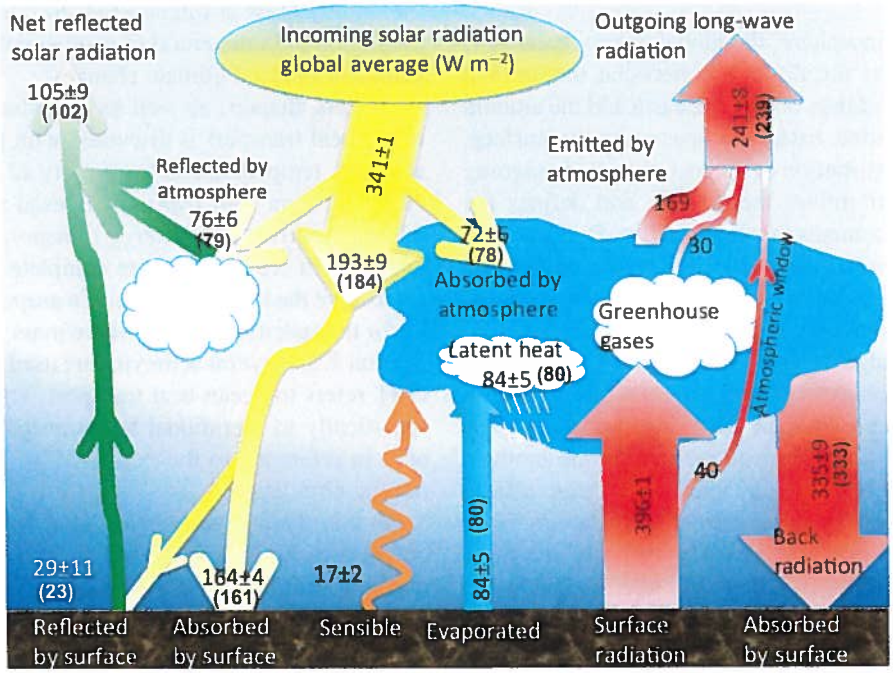

FIGURE 29.1 Global annual mean energy budget including shortwave and longwave radiation, and latent and sensible heat fluxes based on CERES (Clouds and the Earth's Radiant Energy System) data for the period March 2000 to May 2004. Values are the means and standard deviations of the four products compared in Trenberth et al. (2009). Values in parenthesis are the Trenberth et al. estimates where they differ from the mean (Units Wm^{-2}).

longwave radiation, evaporation (latent heat of vaporization), and conduction (sensible heat transfer).

The orientation of the earth to the sun causes the magnitude of net incoming shortwave solar radiation to be greatest near the equator (>300 Wm^{-2}) where it dominates the radiation budget at the top of the atmosphere, and least near the poles (<100 Wm^{-2}) where net upward longwave radiation dominates (Figure 29.2a). This configuration results in a tropical surplus and polar deficit in energy. The equator-to-pole difference in incoming radiation exceeds the equator-to-pole difference in upward radiation. This asymmetry is largely due to differences in absorbed radiation that are caused by the equator-to-pole gradient in albedo (Enderton and Marshall, 2009). According to climate models, there is maximum poleward heat transport (5.6 ± 0.8 PW in the northern hemisphere and -5.3 ± 1.1 PW in the southern hemisphere, 1 PW $= 1 \times 10^{15}$ W) at approximately 35° latitude in each hemisphere (Donohoe and Battisti, 2012). Observational estimates are consistent, if a little higher, at 5.9 ± 0.3 PW in the northern hemisphere and -5.9 ± 0.5 PW in the southern hemisphere (Fasullo and Trenberth, 2008). As a consequence, equatorward of this latitude there would be a net warming, and poleward, a net cooling, if the atmosphere and ocean did not provide the poleward transport of energy necessary to offset the imbalance (Figure 29.2d). Both regimes contribute, but here we focus on the ocean's role in the process.

1.2. Energy Balance at the Ocean Surface

The energy budget at the sea surface is a combination of the four components: net short and longwave radiation (e.g., Figure 29.2b), and net latent and sensible heat flux (e.g., Figure 29.2c). The term shortwave radiation is often used to describe the ultraviolet, visible, and infrared wavelengths (0.2–5 μ) of incoming solar energy, whereas longwave radiation is often associated with the infrared (5–200 μ) emitted by the cooler earth. However, it should be kept in mind that upward and downward components of both longwave and shortwave radiation exist within the energy budget below the top of the atmosphere (Figure 29.1).

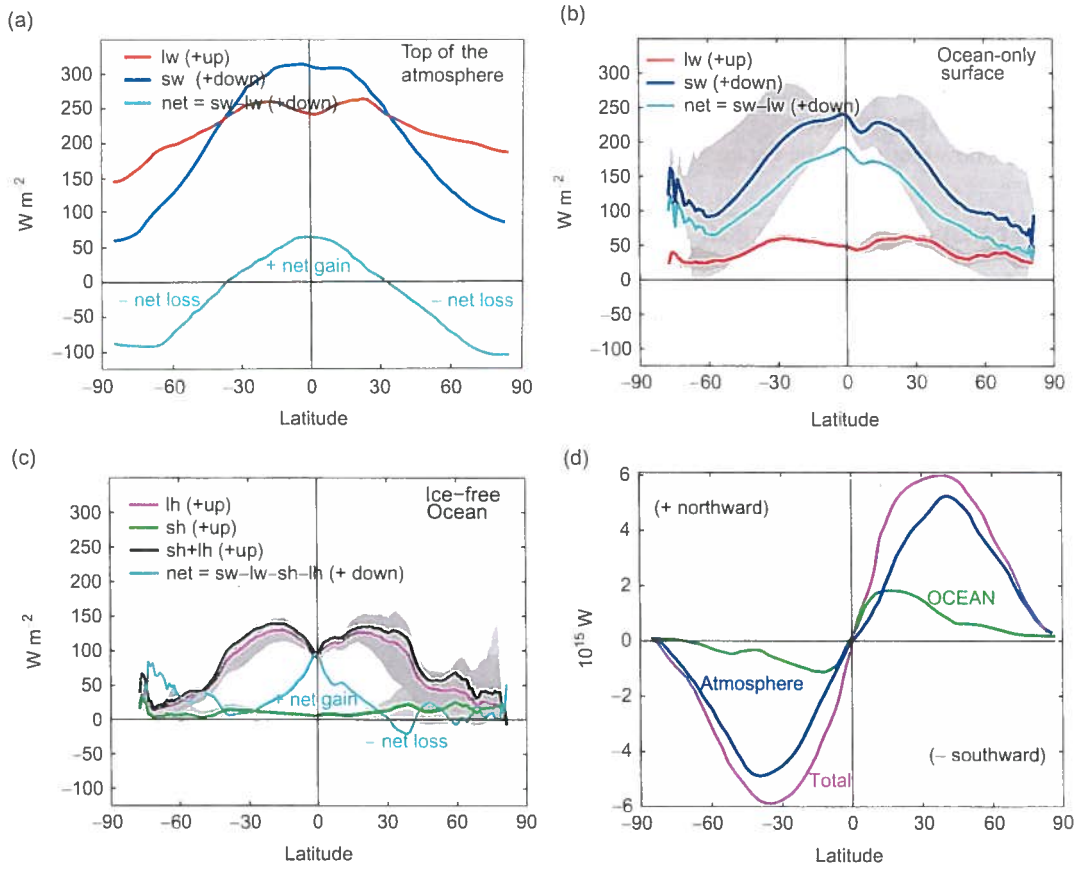

FIGURE 29.2 Components of the energy balance: (a) zonally averaged estimates of annual mean longwave (lw), shortwave (sw) and net (=sw – lw) radiation at (a) the top-of-the-atmosphere (estimates from Hatzianastassiou et al., 2004) and (b) the ocean surface (ISCCP data 1984–2007); (c) zonally averaged annual mean estimates of latent (lh), sensible (sh), latent + sensible and net (=sw – lw – lh – sh, postive down) heat flux. Gray shading illustrates range in monthly average values (OAFlux data from 1958 to 2007. Note this product does not balance globally—see text. Ocean heat flux estimates courtesy of L. Yu) (Units Wm^{-2}); (d) annual mean energy transport by the atmosphere (blue), ocean (green), and atmosphere + ocean (purple). Atmospheric and net values are based on the National Centers for Environmental Prediction-National Center for Atmospheric Research reanalysis, the Earth Radiation Budget Experiment and Global Ocean Data Assimilation System. The ocean curve is a residual estimate (Units PW). *Adapted from Fasullo and Trenberth (2008).*

At the surface of the ocean (Figure 29.2b), the shape of the curve describing the net incoming shortwave radiation is similar to the top-of-the-atmosphere global average (Figure 29.2a). Both imply greater warming at low latitudes than at high latitudes. Latent and sensible heat fluxes from the ocean are large over WBC regions (e.g., Yu et al., 2004). While the influence of subtropical trade winds is clear in the zonally averaged latent fluxes (Figure 29.2c, magenta curve), it is less obvious in the sensible fluxes which show maximum loss in the northern high latitudes (Figure 29.2c, green curve). Loss of energy from the ocean through sensible and latent heat fluxes reduces the magnitude of the net radiation (Figure 29.2c, cyan curve).

Without oceanic transport of energy from the equator to the poles, the global energy balance could not be maintained. Although this unidirectional transport (Figure 29.2d) is clearly implied by the top-of-the-atmosphere radiation distribution (e.g., Figure 29.2a and d), poleward movement of energy in the ocean is by no means ubiquitous (Figure 29.3). Restricted by land and topography, OHT maintains a complex relationship of feedbacks with the atmosphere that influences both the temperature and dynamics within and between the basins. The details of how energy is moved within the individual ocean basins and how it is exchanged between basins are therefore fundamental to our understanding of how ocean energy balances are maintained and how they might be vulnerable to change.

1.3. Heat Transport in the Ocean

The ocean transfers heat from one location to another by transporting waters of different temperatures in opposite directions. Through the dedicated efforts of the ocean-going research community to collect *in situ* full-depth observations in the late twentieth century, estimates of mean basin-scale circulation and MHT have been much improved. By way of introduction to these estimates, we begin here with a brief description of geographical patterns of MHT.

There is a prevailing pattern (Figure 29.3d) of northward MHT throughout the Atlantic Ocean. In the southern hemisphere, this heat transport is composed of northward flow of warm upper and intermediate layer waters entering the basin from the Agulhas region and Drake Passage (Beal et al., 2011; Garzoli and Matano, 2011; Rintoul, 1991; Weijer et al., 2002) (see Chapter 19) and southward flow of North Atlantic Deep Water (NADW) (see Chapter 10). In the North Atlantic, poleward MHT is carried by the relatively warm shallow western boundary current (WBC) and cooler southward return (NADW and abyssal overflow waters) both in the deep western boundary current (DWBC) and the interior. It is the loss of heat from the northward flowing surface waters to the atmosphere along their path throughout the Atlantic that preconditions the deep overturn in the sub-Arctic seas and southward return of cooler waters (Talley, 2003) (see Chapter 13).

In the Indian and Pacific basins, MHT is poleward. In the southern Indo-Pacific (Figure 29.3c), it is dominated by southward transport in the Indian Ocean (Figure 29.3b) supported mainly by a warm upper layer (but, not necessarily surface) export from the tropics of both basins and cooler inflow of Lower Circumpolar Deep Water (LCDW) from the Southern Ocean. Unlike Atlantic MHT, which is predominantly supported by thermohaline overturn, North Pacific MHT (Figure 29.3a), is dominated by the relatively shallow wind-driven gyre circulation and the temperature difference between the northward flowing WBC and the interior return (Bryden et al., 1991; Wijffels et al., 1996).

The simplicity of the above descriptions belies the complexity of the system and the many uncertainties that remain in our understanding of OHT. These uncertainties will be discussed in the context of the estimates themselves in the next two sections. Section 2 provides a basic description of indirect (Section 2.1) and direct (Section 2.2) techniques used to calculate MHT. Section 3 is a more detailed presentation of the resulting estimates that were briefly described earlier. There is an intended focus on the direct, *in situ*, non-numerical model-based estimates. For more discussion on indirect estimates, the reader is directed to Chapter 5 and detailed discussion of state estimates and reanalyses are provided in Chapters 21 and 22.

2. CALCULATION OF OCEAN HEAT TRANSPORT

While a variety of different techniques have been used to assess the role oceans play in the global energy balance, historically speaking, estimates of OHT fall into one of three categories: bulk formula calculations, residual calculations, and direct calculations. The first two methods produce what are considered indirect OHT estimates, as they do not require ocean water column observations. The third method is considered direct because it uses observations of both water temperature and velocity to estimate OHT.

2.1. Indirect Ocean Heat Transport Estimation

The main advantages of indirect methods are that they are capable of providing both global coverage and long, high-resolution, timeseries estimates of OHT. Their disadvantage is that they tend to contain strong regional biases that are not easily removed and can result in large uncertainties in OHT.

- Bulk formulae estimates use observations of radiation, air–sea freshwater and gas exchange, air and sea surface

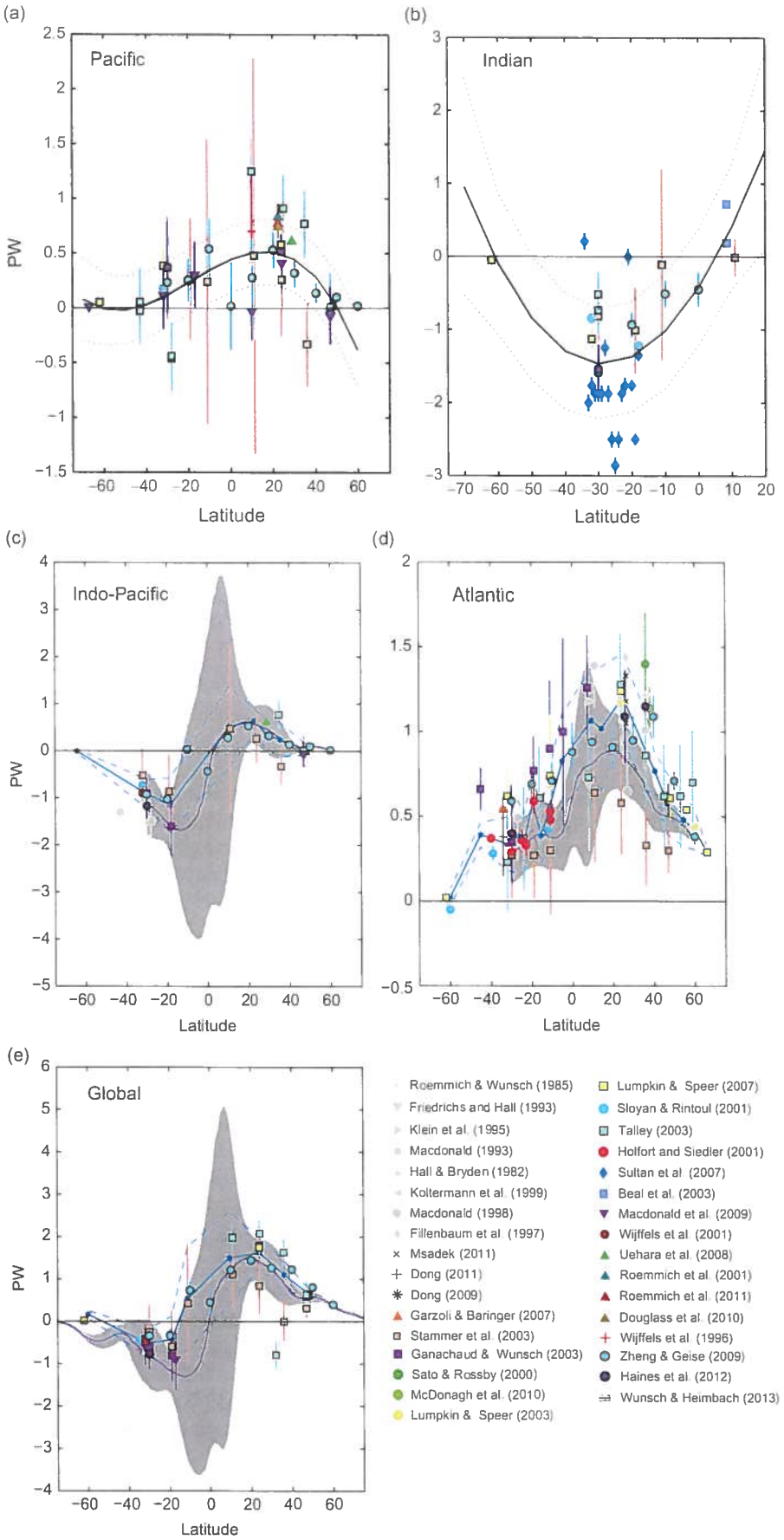

FIGURE 29.3 Estimates of meridional heat (PW)/temperature (PWT) transport for (a) Pacific, (b) Indian, (c) combined Indo-Pacific, (d) Atlantic, and (e) global ocean. Light gray and color markers indicate estimates from publications prior to and later than 2000, respectively. Values in (a) and (b) affected by ITF have been normalized to a 10 Sv throughflow. In (a–b), the thin solid and dashed lines represent a polynomial fit through the data points and the standard deviation of uncertainties. In (c–e), solid and dashed blue lines indicate the mean and standard deviation from Table 29.5. An illustration of the range in seasonal cycles is provided by the dark gray shading representing the standard deviation of the monthly ECCO-Production version 4 (ECCO-GODAE follow-on), global bi-decadal (1992–2010) state estimate (Wunsch and Heimbach, 2013).

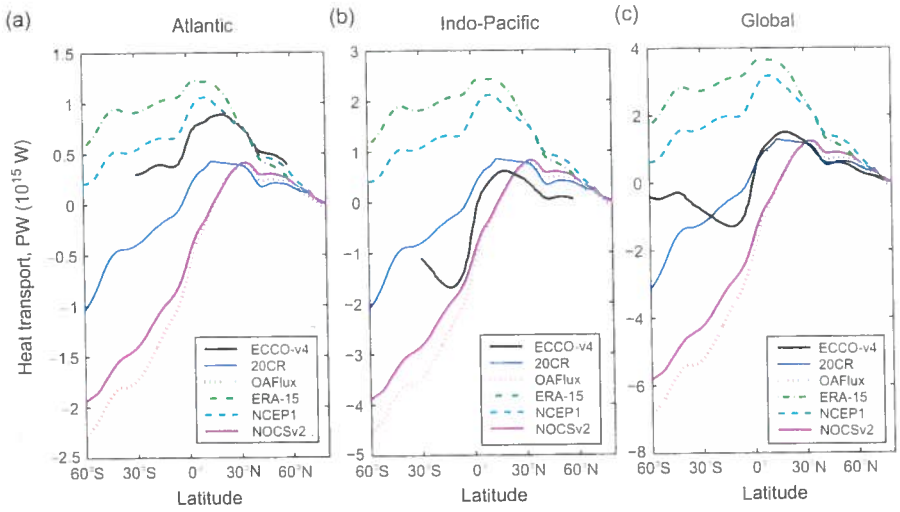

FIGURE 29.4 Meridional heat flux based on different flux products computed by southward integration for (a) the Atlantic, (b) the Indo-Pacific, and (c) the global ocean. The 20CR, OAFlux-ISCCP, ERA-15 (Gibson et al., 1997) and NOCSv2 products and references are listed in Table 29.1. NCEP1 is the original 40-year reanalysis climatology (Kalnay et al., 1996). The large spread away from 0 PW at the southern end of the integration is indicative of the various model biases. We have opted not to remove values representing the global bias from these curves under the assumption that had the individual authors understood these biases well enough to remove them, they would have done so. Please note the different vertical axis limits in each panel.

temperatures, wind speed, etc., along with equations that include empirical coefficients to calculate estimates of each of the four components of the surface energy budget (short and longwave radiation and latent and sensible heat fluxes). Air–sea heat fluxes computed globally are balanced by ocean heat storage and divergence of OHT. Assuming that there is no regional storage of heat within the ocean, the component fluxes can be integrated from north to south to obtain estimates of the OHT necessary to balance the loss or gain through air–sea exchange.

- Residual estimates use atmospheric energy transport estimates calculated from meteorological observations subtracted from the observed top-of-the-atmosphere energy budget to obtain the ocean transport component necessary to provide a balanced budget. The disadvantage of this technique is that any noise in the atmospheric energy budgets is propagated to the OHT estimates.

Bulk formulae parameterizations have steadily improved since the 1990s, from the 30–40 Wm^{-2} global mean uncertainties (da Silva et al., 1994; Josey et al., 1998; Large et al., 1997) that integrated to produce MHT uncertainties of 0.5 PW (1 PW $= 1 \times 10^{15}$ W) or more. Major steps forward included the use of global satellite observations and application of inverse methods that allowed regional parameterizations. Yu et al. (2004) looked to improve estimates using a variational objective analysis, and although they still found a large (30 Wm^{-2}) global imbalance, regional estimates agreed well with direct estimates outside the tropics (Macdonald et al., 2009; Yu et al., 2008). The implied MHT for several commonly available net surface flux products is shown in Figure 29.4. Improvements have also been derived from satellite time series that now span more than two decades. With adjustments, Large and Yeager (2009) find a climatological, global mean air–sea heat flux of 2 Wm^{-2}. Nevertheless, regional uncertainties remain as large as 40 Wm^{-2}. For more detail on where these uncertainties arise in the currently available products, see Chapter 5. Despite the issues with uncertainties, an important advantage to bulk formulae calculations of OHT is that they can provide times series for investigation of interannual variability (Section 5). It is also a technique that can be tuned to specific data sets, observations, or regional dynamics.

Residual methods have also been greatly improved by the global observations afforded by satellite technology including radiation and atmospheric temperature and moisture datasets. Other improvements include separation of land and sea domains, global models that have improved the accuracy and detail of estimates of nonradiative flux components, and improved understanding of the annual and interannual variations in the atmospheric energy budget. Nevertheless, satellite observations still find imbalances in the global mean top-of-the-atmosphere energy budget (6.4 Wm^{-2} from CERES (Trenberth et al., 2009)) that suggest warming greater than that expected from the anthropogenic increase in greenhouse aerosols alone (1.6 ± 0.3 Wm^{-2} (Hansen et al., 2011)). Likewise, models do not generally provide a radiative balance at the top of the atmosphere. Most predict radiative heating (Hatzianastassiou et al., 2004; Loeb et al., 2002; Wang et al., 2011). Further, the variety of observations now available are not easily synthesized into

internally compatible data sets (Bourras, 2006; Brodeau et al., 2010; Garnier et al., 2000), which are needed to drive simulations or validate model results.

Looking at the range in estimates (Bourras, 2006; Liu et al., 2011b; Smith et al., 2011; Trenberth et al., 2009, 2011) for the various top-of-the-atmosphere and surface components of the energy budget from the extensive set of currently available flux products (Table 29.1) provides some measure of present-day uncertainty in the individual components. However, Trenberth et al. (2009) point out that the spread of estimates exaggerates the actual uncertainties, since many of the weaknesses in the individual products are understood (Berry and Kent, 2009; Moore and Refrew, 2002; Siqueira and Nobre, 2006; Smith et al., 2011; Uppala et al., 2005). For this reason, there is no one flux product that is best suited for all applications (Berry and Kent, 2009; Smith et al., 2011; Tomita et al., 2010). According to Trenberth et al. (2009), global top-of-the-atmosphere components are known to within about 3%, surface reflected solar radiation, latent heat of evaporation and net longwave radiation are good to about 10%, and other surface components to about 5% (see Figure 29.1 to convert percentages to approximate values in Wm^{-2}). They consider the largest remaining uncertainty to be due to clouds and the biased estimates of downward longwave radiation (back radiation in Figure 29.1). Adjustments of flux products have been able to reduce regional rms differences with *in situ* surface estimates to about 1–2 Wm^{-2} (Grist and Josey, 2003). However, global biases in the individual components of radiation remain on the order of 5–30 Wm^{-2} (Bourras, 2006; Large and Yeager, 2009; Liu et al., 2011a; Trenberth and Smith, 2009; Wang et al., 2011). These biases are particularly large in the Southern Ocean due to the sparsity in both time and space of directly observed surface meteorological data. The lack of Southern Ocean data is largely due to an absence of ship tracks. The result is a large spread in indirectly estimated MHT (Figure 29.4), particularly in the Southern Hemisphere.

In summary, over the past 10 years, there has been great improvement in flux products. Time series, multiple decades in length, are becoming the norm, making climate analyses feasible. To understand and reduce uncertainties, there remains a need for metrics and comparison, both to observations and among products. When it comes to estimating OHT, lack of direct observations in the Southern Ocean for comparison and constraint is likely the most difficult issue we face in coming years. Further details on surface fluxes and flux products can be found in Chapter 5.

2.2. Direct Ocean Heat Transport Estimation

Direct estimates of OHT are based on observations of ocean water column temperature and on either direct or inferred velocity estimates that are also derived from observations. The general equation for the calculation of heat transport perpendicular to a hydrographic transect (Bryan, 1962) is:

$$\int\int \rho(x,z)C_p(x,z)\Theta(x,z)v(x,z)\mathrm{d}x\mathrm{d}z, \qquad (29.1)$$

where ρ represents density, C_p the specific heat of water at constant pressure, which is a function of temperature (T) and salinity (S), Θ the potential temperature, v the velocity perpendicular to the transect, and x and z the distance and depth coordinates. Density, C_p, Θ, and v are all functions of temperature, salinity and pressure and v is typically computed as a geostrophic balance with corrections for ageostrophic motion like Ekman transport included. The integral is taken vertically and horizontally across a slice of the ocean where a mass balance,

$$\int\int \rho(x,z)v(x,z)\mathrm{d}x\mathrm{d}z = 0 \qquad (29.2)$$

exists.

It is understood that to compare estimates of heat transport there must be an underlying mass balance, otherwise a change in units such as from °C to °K would create a change in the magnitude of the heat transport estimate. To make the distinction, where mass balance is either not possible or not sensible, heat transport is referred to as *temperature transport*. It is referenced to °C and is accompanied by a net mass or volume transport estimate. Following Talley (2003), temperature transport is reported in units of PWT (PW with the T reminding the reader that the value is a nonmass-balanced temperature transport). Positive values indicate northward (and eastward) flow.

Estimates using Equations (29.1) and (29.2) are typically constructed from temperature, salinity, and pressure observations from hydrographic transects using a variety of techniques described in basic physical oceanography texts. One specific goal of the 1990s World Ocean Circulation Experiment (WOCE) was to obtain a quantitative description of the circulation of heat throughout the global ocean. Previously, the historical hydrographic record contained few basin-scale transects, and even fewer transects which conformed to any particular standard of measurement quality. The WOCE program expanded ocean observations to include multiple high-quality hydrographic zonal sections in each of the ocean basins, with well-defined best practices and standards. Supplemented by transect data from other programs that occurred from the late 1980s through the WOCE-period, a 10-year "synoptic" observational data base was obtained, which could be used to quantify the ocean component of MHT. The WOCE program included observations of direct velocity and temperature in strongly temporally varying boundary current regions, as well as interior absolute velocity measurements on some of the transects from Acoustic Doppler Current

TABLE 29.1 Some Currently Available Global Flux Products that Can be Used to Estimate OHT

Product	References	Comment
SOC/NOC1.1	Grist and Josey (2003)	COADS air–sea flux VOS climatology constrained by hydrography
	http://iridl.ldeo.columbia.edu/SOURCES/.SOC/.GASC97/.dataset_documentation.html	
ERA-15	Bromwich and Wang (2005)	ECMWF 15-year reanalysis, daily/monthly (1978–1994)
	http://www.ecmwf.int/research/era/ERA-15/	
ERA-40	Uppala et al. (2005)	ECMWF 40-year reanalysis, daily/monthly (1957–2002)
	http://www.ecmwf.int/products/data/archive/descriptions/e4/index.html	
JRA-25	Onogi et al. (2007)	Japanese 25-year reanalysis, 6 hourly (1979–2004)
	http://jra.kishou.go.jp/JRA-25/AboutJRA25_en.html	
OAFlux	Yu et al. (2008)	Objective analysis, near real-time reanalysis, daily/monthly (1958 on)
	http://oaflux.whoi.edu/index.html	
CORE v2	Large and Yeager (2009)	Air–sea flux components from atmospheric state fields (1949 on)
	http://rda.ucar.edu/datasets/ds260.2/	
NOCS v2	Berry and Kent (2009)	Air–sea flux from ICOADS (1973–2009)
	http://www.noc.soton.ac.uk/noc_flux/noc2.php	
ERA-I	Dee et al. (2011)	ECMWF near real-time reanalysis, daily/monthly (1979 on)
	http://www.ecmwf.int/products/data/archive/descriptions/ei/index.html	
MERRA	Bosilovich et al. (2011)	Satellite era daily reanalysis of GEOS-5 (1979 on)
	http://gmao.gsfc.nasa.gov/merra/	
CFSR	Saha et al. (2010) and Wang et al. (2011)	NCEP daily reanalysis including trace gases (1979 on)
	http://cfs.ncep.noaa.gov/	
20CR	Compo et al. (2011)	NOAA Sub-daily/daily/monthly (1870–2010)
	https://climatedataguide.ucar.edu/category/data-set-variables/reanalysis/noaa-20cr	
HOAPS 3.2	Fennig et al. (2012)	Satellite-only based climatology, 6 hourly/monthly (1987–2008)
	http://www.hoaps.zmaw.de/	
J-OFURO	Dee et al. (2011)	Satellite based climatology, daily/monthly (1988–2006)
	http://dtsv.scc.u-tokai.ac.jp/j-ofuro/dataset_information.html	
GSSTF 3	Shie et al. (2012)	Satellite based climatology, daily/monthly (1998–2008)
	http://disc.sci.gsfc.nasa.gov/datareleases/gsstf-version	
HOAPS 3.2	Fennig et al. (2012)	Satellite-only based climatology, 6 hourly/monthly (1987–2008)
	http://www.hoaps.zmaw.de/	

HOAPS, Hamburg Ocean Atmosphere Parameters and Fluxes from Satellite Data; SOC, Southampton Oceanography Centre; NOC, National Oceanography Centre; COADS, Comprehensive Ocean-Atmosphere Data Set; VOS, volunteer ship of opportunity; ECMWF, European Centre for Medium Range Weather Forecasts; CORE, Common Ocean Reference Experiment; MERRA, Modern-Era Retrospective Analysis for Research and Applications; GEOS, Goddard Earth Observing System data assimilation; CFSR, Climate Forcing System Reanalysis; OFURO, Japanese Ocean data Flux sets with Use of Remote sensing Observations; GSSTF, Goddard Satellite-based Surface Turbulent Fluxes. For further details and data, see the links provided. Also details on comparative features can be found in the climate reanalysis data guide provided by the National Center for Atmospheric Research: http://climatedataguide.ucar.edu/.

TABLE 29.2 Comparison of the BBH and SOV Decompositions from Talley (2003) Provided as Percentages of the Total Heat Transport According to Each Method Across 5 Zonal Sections Representing the Northern and Southern Hemisphere Subtropical Gyres

		SOV Decomposition (% of Total)			BBH Decomposition (% of Total)		
Section	Total Heat Transport (PW)	ITF/BS Throughflow (%)	SOV (%)	Int./Deep Overturn (%)	Barotropic (%)	Horizontal (%)	Baroclinic (%)
Atlantic 24°N	1.28	−2	32	**70**	−3	9	**94**
Pacific 24°N	0.81	17	**68**	15	4	**60**	37
Atlantic 32°S	0.23	−10	−52	**162**	−12	−108	**220**
Pacific 28°S	−0.43	−14	57	57	**52**	36	11
Indian 32°S	−0.59	12	**47**	41	−43	45	**98**

Positive percentages indicate transport in the direction of the total. Bold face values indicate the dominant components at individual latitudes according to each of the two methods.

Profilers (SADCP and LADCP, ship and lowered, respectively), and volunteer ship of opportunity repeat temperature profiles (Festa and Molinari, 1992). Over the last decade, the WOCE data set has been expanded to include repeats of many of these transects through the international efforts of the hydrographic component of the Climate Variability and Predictability (CLIVAR) program, which is now being coordinated through Global Ocean Ship-based Hydrographic Investigations Program (GO-SHIP) (see Chapter 3). Along with estimates at individual latitudes, many of these observations have been used in data syntheses that can compute or correct estimates of both heat transport and air–sea heat fluxes such as the inverse box model solutions of Ganachaud and Wunsch (2003), Lumpkin and Speer (2007), and Macdonald et al. (2009).

A major roadblock to calculating meridional heat transports from long-line hydrographic transects lies in calculating reliable estimates of the absolute velocity field. A variety of methods are used to estimate the unknown barotropic velocities inherent in velocity fields based on hydrography and these methods vary considerably by region and investigator. They will not be discussed here as they are described in most introductory texts. A major step forward was taken when Wunsch (1977) introduced the physical oceanography community to the inverse technique (Wiggins, 1972) for determining least squares (Lawson and Hanson, 1974) best-estimate solutions for these unknown velocity corrections. Initially used on single transects, it quickly became popular as a technique for combining observations from multiple transects and different data sets (Wunsch, 1996). The two main advantages of this method are that it encourages users to state all assumptions clearly, and when possible, produces solutions consistent with the stated assumptions. Describing the inverse method simply, observations are used to write a set of constraint equations (i.e., physical assumptions about dynamics, conservation, and uncertainties), which are formulated as an eigenvalue problem that can then be solved in a variety of ways. It was this type of formulism that eventually led to state-estimates (Chapters 21 and 22).

In the next section, we take a basin-by-basin look at some of the OHT estimates arising from the now diverse set of observations and calculation techniques.

3. OBSERVATION-BASED ESTIMATES OF OCEAN HEAT TRANSPORT

Using a hypothetical-closed overturning circulation, Jung (1952) made the remarkably accurate calculation that at 30°N the Atlantic Ocean could support a MHT of 3×10^{14} gm-cal s^{-1} (about 1.3 PW in modern units). He confirmed the result with observations from the Wüst and Defant (1936) Meteor Atlas. Half a century later, Bryden and Imawaki (2001) reported on a single global synthesis that estimated MHT across 15 zonal pre-WOCE transects (Macdonald, 1998) and was able to include 6 WOCE-era estimates in the Atlantic (Bacon, 1997; Holfort and Siedler 2001; Klein et al., 1995; Lavin et al., 1998; Saunders and King, 1995; Speer et al., 1996). In the intervening decade, the WOCE and CLIVAR programs, and volunteer ship of opportunity XBT programs have provided a relative plethora of ocean observations with which to investigate OHT (Figures 29.3 and 29.5, Tables 29.3–29.5). These new observations and analyses have provided further insights into our understanding of ocean heat transports, but have not yet answered many of the open questions. In the following subsections, we discuss direct steady-state OHT estimates in light of these estimates. Here and throughout this chapter, results are considered to be inconsistent (i.e., significantly different) when the stated values

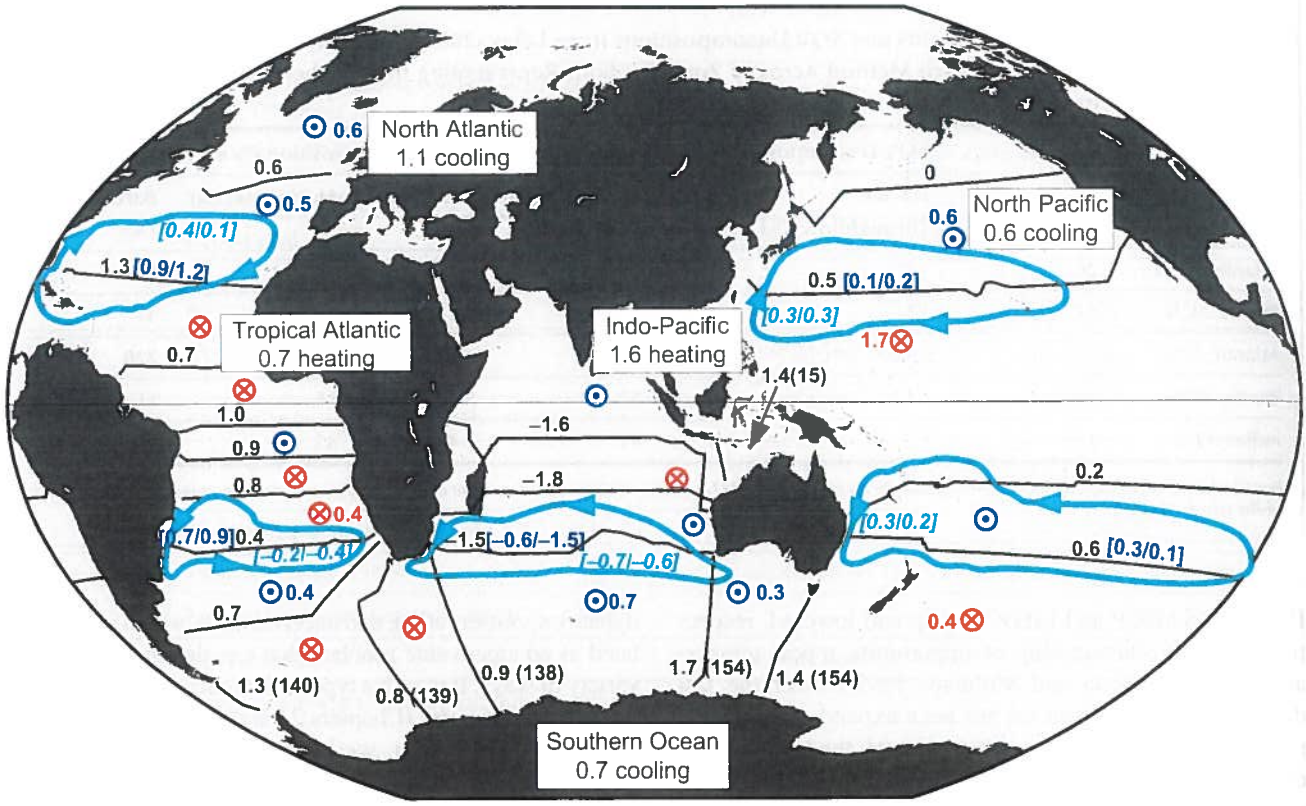

FIGURE 29.5 Estimates of ocean heat transport (black) with significant net volume transport in parentheses, convergence (gain of heat from the atmosphere) and divergence (loss of heat to the atmosphere) from Ganachaud and Wunsch (2000) (GW00). Red arrow tails and blue heads indicate convergence and divergence, respectively and estimated magnitudes are shown where they differ significantly from zero. Full basin convergence estimates are provided in boxes. Black lines indicate the location of hydrographic sections used by GW00 in their WOCE-era global inversion. Estimated uncertainties are provided in Tables 29.3 and 29.4. Values delineated by square brackets in cyan and blue are the estimated components of GW00's MHT at 24°N and 30°S due to gyre and overturn, respectively, based on Table 29.3. These components, separated by a "/," are the SOV shallow subducting overturn/BBH horizontal gyre components (cyan), and the SOV deep overturn/BBH baroclinic components (blue). The associated anticyclonic wind-driven gyre circulation is shown schematically in light blue with directional arrows according to T03 based on the predominantly pre-WOCE adjusted geostrophic fields of Reid (1994, 1997). Positive values indicate northward and eastward flow. Units (PW, PWT in ACC). *Adapted from both GW00 and T03.*

plus/minus the associated uncertainty reported by the authors do not overlap.

3.1. Atlantic

The Atlantic Ocean, the first place where MHT was estimated (Jung, 1952; Sverdrup, 1957), has arguably become the best-observed basin in terms of both mass and heat transport (Figure 29.3d). Throughout much of the Atlantic, the vertically integrated overturn and the temperature difference between surface/upper layer waters and the southward flowing NADW are primarily responsible for the northward transport of heat in both hemispheres (Figures 29.3a and 29.5, and see detailed discussion of particular estimates in Bryden and Imawaki, 2001).

Beginning our discussion in the north, Lumpkin and Speer (2007) estimate a MHT across 66°N of 0.29 ± 0.02 PW. They used five different surface air–sea flux products (da Silva et al., 1994; Grist and Josey, 2003; Josey et al., 1998; NCEP/NCAR and ERA-15) in their ocean inverse box model. They found that none of these products were capable of supplying sufficient heat loss to the atmosphere to allow formation of observed rates of Denmark Strait and Faroe Bank overflow and Antarctic Bottom Water (AABW) transport across 62°S. They reasoned that the models were unable to resolve the strong air–sea exchange that occurs at small scales (e.g., in narrow boundary currents, leads, and polynas that are common) at high latitudes. This observation may explain the disagreement between their estimate of MHT across 66°N and that of various flux products (Figure 29.4).

At 45–50°N, there are numerous MHT estimates. They consistently suggest a northward heat transport of about 0.6 PW. The weighted mean of the estimates in Table 29.3 (including only those estimates with uncertainties), and the rms uncertainty is 0.58 ± 0.24 PW (column 13). The average is lowered by the assimilation estimate of Stammer et al. (2003) who noted that their ocean MHT estimates generally tended to fall below those made directly from the observations, hypothesizing that the 2° horizontal resolution ECCO model used at that time did not well resolve either WBCs or the temperature difference

TABLE 29.3 Atlantic Ocean MHT Estimates, Predominantly Based on Observations (Lower Case Superscripts) with Indirect and Model Estimates (Upper Case Superscripts) Included Where Calculated by the Same Authors

Atlantic Meridional Heat Transport Estimates (PW)												
Latitude	WH13	ZG09	LS07	T03	GW03	SE03	Other Estimates					Mean
66°N			0.29 ± 0.02					0.30 ± 0.03[l]				0.29 ± 0.03
59–60°N		0.38 ± 0.04		0.7				0.44 ± 0.03[l]				0.43 ± 0.18
53–56°N	0.43 ± 0.05		0.54 ± 0.11	0.62								0.48 ± 0.19
45–48°N	0.50 ± 0.09	0.71 ± 0.05	0.61 ± 0.13	0.62	0.60 ± 0.09	0.30 ± 0.13	0.65 ± 0.25[hh]	0.60 ± 0.04[l]	0.27 ± 0.15[a]	0.62 ± 0.11[a]	0.53 ± 0.12[a]	0.58 ± 0.24
40–41°N		1.09 ± 0.12					0.50 ± 0.10[n]					0.77 ± 0.11
36–38°N	0.62 ± 0.17			0.86		0.33 ± 0.23	1.01 ± 0.26[hh]	1.14 ± 0.12[l]	0.47 ± 0.24[a]	1.29 ± 0.17[a]	0.70 ± 0.15[a]	0.88 ± 0.22
							0.8[n]	1.4 ± 0.3[o]	1.15[ll]			
24–26°N	0.84 ± 0.21	0.95 ± 0.14	1.24 ± 0.25	1.28	1.27 ± 0.15	0.58 ± 0.30	1.07 ± 0.26[hh]	1.17 ± 0.08[j]	1.38 ± 0.29[a]	1.48 ± 0.20[a]	1.54 ± 0.19[a]	1.20 ± 0.27
							1.33[h]	1.05–1.18[B]	1.44 ± 0.33[e]	1.2[dkl]	1.21 ± 0.34[ll]	
							1.2 ± 0.3[p]	1.27 ± 0.26[q]	1.2 ± 0.26[q]	1.33 ± 0.26[q]	1.51 ± 0.39[hh]	
							1.33 ± 0.40[cc]	1.09 ± 0.27[ll]				
15°N	0.87 ± 0.31						1.22 ± 0.42[s]					0.39 ± 0.21
8–11°N	0.82 ± 0.47	0.94 ± 0.15		0.73	1.26 ± 0.31	0.64 ± 0.41	1.39 ± 0.25[hh]	1.1 ± 0.2[r]	1.18 ± 0.52[s]	1.28 ± 0.17[ee]		1.07 ± 0.33
0–5°S	0.40 ± 0.23	0.88 ± 0.17			1.00 ± 0.55			1.00 ± 0.14[ee]				0.83 ± 0.32
11–12°S	0.38 ± 0.20	0.71 ± 0.11	0.74 ± 0.36		0.9 ± 0.4	0.30 ± 0.38	0.89 ± 0.25[hh]	0.69 ± 0.10[l]	0.42 ± 0.05[k]	0.53 ± 0.08[s]	0.48 ± 0.09[s]	0.56 ± 0.26
15–16°S	0.40 ± 0.19			0.16			0.4 ± 0.02[y]					0.39 ± 0.21
19–20°S	0.38 ± 0.18	0.69 ± 0.08			0.77 ± 0.20	0.27 ± 0.25		0.59 ± 0.07[s]				0.58 ± 0.17
23–25°S	0.32 ± 0.17			0.37			0.33 ± 0.25[hh]	0.36 ± 0.06[s]	0.33 ± 0.06[s]			0.34 ± 0.19
27°S	0.31 ± 0.18						0.49 ± 0.25[hh]					0.39 ± 0.18
30–34°S	0.30 ± 0.20	0.59 ± 0.07	0.62 ± 0.16	0.23	0.35 ± 0.15	0.27 ± 0.25	0.55 ± 0.13[d]	0.38 ± 0.23[C]	0.29 ± 0.05[s]	0.22 ± 0.08[z]		0.34 ± 0.18
							0.25 ± 0.12[t]	0.3 ± 0.02[y]	0.40 ± 0.28[ll]			
45°S					0.66 ± 0.12		0.28 ± 0.04[k]	0.43 ± 0.08[z]	0.5 ± 0.1[dd]	0.37 ± 0.02[s]		0.39 ± 0.08
57–62°S			0.02 ± 0.05				−0.03 ± 0.25[hh]	−0.05 ± 0.01[k]				−0.03 ± 0.01

Columns 2–7: Global estimates from five publications, WH13—Wunsch and Heimbach (2013) uncertainties are a measure of the seasonal signal; ZG09—Zheng and Giese (2009) SODA Reanalysis (1958–2004) standard deviation calculated with annual cycle was removed; LS07—Lumpkin and Speer (2007); T03—Talley (2003) uncertainties 0.2–0.3 PW; GW03—Ganachaud and Wunsch (2003); SE03—Stammer et al. (2003). Columns 8–11: Section, basin, or hemisphere specific and pre-2000 estimates. Superscripts: [a]Koltermann et al. (1999) 1957–59, 1981–82, 1992–93 data from left to right, respectively; [b]Msadek (2011); [c]Dong et al. (2011); [d]Garzoli and Baringer (2007); [e]Fillenbaum et al. (1997); [f]Roemmich et al. (2001); [g]Roemmich and Gilson (2011); [h]Uehara et al. (2008); [i]McDonagh et al. (2010); [j]Lumpkin and Speer (2003); [k]Sloyan and Rintoul (2001) (ITF = 7.4–10.3); [m]Beal et al. (2003) Just the Arabian Sea; [n]Macdonald et al. (2009); [o]Sato and Rossby (2000); [p]Hall and Bryden (1982); [q]Lavín et al. (1998) 1957, 1981, 1992 data from left to right; [r]Friedrichs and Hall (1993); [s]Holfort and Siedler (2001); errors do not include ~0.24 PW unresolved uncertainty associated with wind stress and temporal variability. [t]Rintoul (1991); [u]Roemmich and McCallister (1989); [v]Bryden et al. (1991); [w]Wijffels et al. (2001); [x]Klein et al. (1995); [y]Macdonald (1993)(ITF = 10); [z]McDonagh and King (2005); [aa]Saunders and King (1995); [bb]Lavín et al. (2003); [cc]Johns et al. (2011); [dd]Roemmich and Wunsch (1985) data from 1957 and 1981; [ee]Marin (1998); [ff]Molinari et al. (1990); [gg]Wijffels et al. (1996); [hh]Macdonald (1998)(ITF = 8.1); [ii]Hobbs and Willis (2012) Argo; [jj]Haines et al. (2012) UR025.3 Reanalysis (1993–2009). Column 13: Weighted mean and rms uncertainty of OHT values in the row.

TABLE 29.4 Same as Table 29.3, but for Indo-Pacific

Indo-Pacific Meridional Heat Transport Estimates (PW)

	WH13	ZG09	LS07	T03	GW03	SE03				
Latitude	ITF = 16.4 ± 3.7	ITF = 15*	ITF = 13.2 ± 1.8	ITF = 8	ITF = 15 ± 3	ITF = 11	Other Estimates			Mean
47–48°N	0.09 ± 0.09	0.10 ± 0.02[+]	0.00 ± 0.07	0.01	0.00 ± 0.05	0.00 ± 0.13	−0.08 ± 0.25[hh]	−0.09[u]	−0.07 ± 0.1[n]	0.04 ± 0.16
35–36°N	0.24 ± 0.39	0.14 ± 0.39[++]		0.77		−0.33 ± 0.38		−0.16[u]		0.24 ± 0.37
29–30°N	0.47 ± 0.52	0.32 ± 0.12						0.61[h]		0.35 ± 0.38
22–24°N	0.55 ± 0.43	0.53 ± 0.16[+++]	0.58 ± 0.35	0.81	0.52 ± 0.20	0.26 ± 0.51	0.45 ± 0.26[hh]	0.83 ± 0.12[t]	0.77 ± 0.12[g]	0.64 ± 0.29
							0.74 ± 0.10[h]	0.41 ± 0.26[n]	0.75[u] ± 0.76[v]	
10–11°N	0.45 ± 2.55	0.28 ± 0.36		1.25		0.47 ± 1.8	0.44 ± 0.25[hh]	0.03 ± 0.26[n]	0.7 ± 0.5[gg]	0.51 ± 1.22
9°N	0.37 ± 3.19						0.19–0.72[m]			
17–20°S	−1.56 ± 0.59	−1.02 ± 0.18			−1.6 ± 0.6	−0.86 ± 0.80	−0.9 ± 0.7[n]			−1.15 ± 0.61
28–32°S[#]	−1.10 ± 0.68	−0.93 ± 0.12	−1.00 ± 0.19	−1.02	−0.9 ± 0.3	−0.52 ± 0.56	−1.34 ± 0.30[hh]	−0.74 ± 0.07[k]	−1.0 ± 0.1[v]	−0.91 ± 0.36
							−1.17 ± 0.37[ll]	−0.90[w]	−0.6 ± 0.4[n]	
62°S			0.00 ± 0.05							

Although some individual basin values have been summed to obtain total Indo-Pacific estimates, no ITF normalization has been performed, for the reason that ITF values are provided in the headers of columns 2–6 and in the caption of Table 29.1 for columns 7–10. *ZG09 average ITF transport is from Carton and Giese (2008). [+]Estimate is for 50°N. [++]Estimate is for 40°N. [+++]Estimate is for 20°N. [#]Pre-WOCE estimates of net Indo-Pacific heat transport across 32°S usually used the 1967 Scorpio 28°S observations in the Pacific Ocean (ITF units $10^6 ms^{-1}$).

TABLE 29.5 Same as Table 29.3 and 29.4, Zonally Integrated at Each Latitude Across all Basins

Global Ocean Meridional Heat Transport Estimates (PW)

Latitude	WH13	ZG09	LS07	T03	GW03	SE03	Other Estimates				Mean
47–48°N	0.58 ± 0.15	[+]0.81 ± 0.04	0.62 ± 0.08	0.63	0.6 ± 0.1	0.60 ± 0.10					0.68 ± 0.15
36°N	0.90 ± 0.50	[++]1.23 ± 0.10		1.63		0.00 ± 0.44					1.11 ± 0.37
24°N	1.42 ± 0.54	[+++]1.44 ± 0.15	1.75 ± 0.19	2.09	1.8 ± 0.3	0.84 ± 0.64					1.62 ± 0.40
8–11°N	1.27 ± 2.94	1.22 ± 0.28		1.98		1.11 ± 0.80					1.50 ± 1.54
10–11°S	−1.28 ± 2.08	0.74 ± 0.20				0.43 ± 1.40					0.55 ± 1.45
19–20°S	−1.18 ± 0.62	−0.33 ± 0.15			−0.8 ± 0.6	0.59 ± 0.84					−0.43 ± 0.61
30–32°S	−0.72 ± 0.77	−0.34 ± 0.11	0.41 ± 0.18	−0.79	−0.6 ± 0.3	−0.25 ± 0.62	−0.7 ± 0.1[y]	−0.46 ± 0.38[w]	−0.46 ± 0.08[k]	−0.77 ± 0.34[ll]	−0.51 ± 0.39
60–62°S	−0.40 ± 0.11		0.02 ± 0.07								0.17 ± 0.09

between WBCs and the interior. The mean estimate is also reduced by the 0.27 ± 0.15 PW estimate from Koltermann et al. (1999). This value was based on the IGY 1957 observations which, as Koltermann et al. point out, had much lower resolution O(100 nm) than more modern estimates. Using data from 1957, 1981, and 1993, they concluded that the differences in their MHT estimates (0.27–0.62 PW) were due to variations in the geostrophic circulation and, in particular, differences in MOC (estimated as 9.2 ± 2.0 Sv (1957), 18.9 ± 1.3 Sv (1981), and 14.7 ± 1.2 Sv (1993), where $1\ \text{Sv} = 1 \times 10^6\ \text{m}^3\ \text{s}^{-1}$). How much these particular MOC estimates are influenced by the details of the observations (resolution, seasonality, etc.) and physical assumptions as opposed to actual decadal changes is not obvious. The wide range of estimates, however, points to the tremendous influence of circulation on MHT and likely explains a great deal about the range in estimates at all latitudes.

At 36°N, the ocean MHT is about 1 PW (weighted mean $= 0.88 \pm 0.22$). Again estimates from the assimilation and the IGY dataset lie at the lower end of the spectrum. Koltermann et al. (1999) would suggest that the latter is for the same reason as at 48°N. Their MOC estimates at this latitude are 7.5 ± 2.2 Sv (spring 1959), 20.1 ± 1.4 Sv (summer 1981), and 12.3 ± 1.2 Sv (fall 1993). Similarly, Sato and Rossby (2000) found that WBC temperature flux at this latitude is dependent upon station density. Using historical hydrography (boundary current data from the early 1930s to the late 1980s), they find a seasonal cycle in heat transport at this latitude with a peak-to-peak range of 0.6 ± 0.1 PW, suggesting the spread seen by Koltermann et al. may also be attributable to a seasonal signal. It should be noted that the global inverse solution of Ganachaud and Wunsch (2000) did not include the 1993 data set used by Koltermann et al. at this latitude because it was not thought to meet WOCE standards. Combining hydrography and ADCP data from the May–June 2005 CLIVAR dataset, McDonagh et al. (2010) find 1.14 ± 0.12 PW crossing 36°N, an estimate higher than, but consistent with, Koltermann's summer 1981 estimate, and inconsistent with both the spring 1957 and fall 1993 estimates. McDonagh et al. determined that as expected the heat transport here is dominated by the overturn: 0.75 PW associated with overturn and a 10 °C temperature difference between the upper 1000 m and the water below and 0.39 PW associated with horizontal transport predominantly in the upper 800 m.

Across the line that lies nominally between 24.5 and 27°N, a diverse assortment of measurement techniques have been applied to the direct estimation of both the MOC and MHT, including repeat hydrography, moorings, XBTs, and most recently, the integrated MOCHA/RAPID array (see Section 5 for time series estimates). As at latitudes to the north, the estimate of WBC transport has been found to be important to MHT estimates, as has the resolution of the particular sections used. The weighted mean of the values in Table 29.3 is 1.20 ± 0.27 PW, which is consistent with the mean estimate from 3.5 years of time series data from the MOCHA/RAPID array (1.33 ± 0.40 PW (Johns et al., 2011)). The range in nonassimilation-based estimates (0.5 PW) is a large fraction of the mean. A portion of the spread is due to the choice by some to use *in situ* cruise surface temperatures and winds, rather than annual means, in calculating the Ekman component of MHT. Lavín et al. (2003) attribute 0.14 PW to what they term "seasonal sampling," referring to MHT calculated using the mean Florida Strait temperature from their 1992 cruise compared to that using an annual mean. The half petawatt spread in values is similar to the 0.6 PW annual range reported by Johns et al. (2011) for the RAPID time series.

At 15°N, the latitude at which indirect estimates would suggest there is a maximum in poleward MHT (Figures 29.2d and 29.4), there is only a single direct estimate (Klein et al., 1995) based on the combination of two pre-WOCE hydrographic lines. The main challenges encountered in directly measuring MHT with hydrography in the tropics are high variability in winds and in the WBC. The geometry near 15°N in the Atlantic further complicates matters because the unique Lesser Antilles Island chain enclosing the Caribbean Sea makes designing a hydrographic section to cleanly measure WBC transport extremely difficult. Klein et al. (1995) report that of the 1.18 ± 0.52 PW and 1.22 ± 0.42 PW at 8 and 14.5°N, respectively, most is associated with the annual mean Ekman transport. Due to the strong seasonal variation in the winds, using seasonal (i.e., *in situ*) estimates of the Ekman components increases these estimates to 1.67 and 1.37 PW, respectively. This result is consistent with Friedrichs and Hall (1993) who found their MHT estimate based on *in situ* winds at 11°N was 0.8 PW, less than the 1.1 ± 0.2 PW estimated as an annual average. Nevertheless, it appears that large seasonal variations in wind-induced heat transport do not necessarily invalidate "steady-state" hydrographic estimates as long as annual average winds are used. This is because while time-mean Ekman mass transports are balanced at relatively shallow depths (explaining their importance to the total heat transport in regions where they are strong), seasonal variations in Ekman transport are compensated by depth-independent flow (Jayne and Marotzke, 2001) that is not measured by hydrography.

Estimates of Atlantic Ocean MHT between 8°N and 5°S have average values of 1.07 ± 0.33 PW and 0.83 ± 0.32 PW northward, respectively, indicating a small O(0.2 PW) cross-hemispheric gradient that is not significantly different from zero. Only the somewhat lower Talley (2003) estimates would indicate otherwise. She predicts a strong significant divergence of $\sim 0.57 \pm 0.3$ PW. It should be noted that the Reid (1994) data set as interpreted by Talley (2003)

offers our only MHT estimate at 8°S. It is southward (−0.22 PW) as is the accompanying estimate at 11°S (−0.38 PW). However, as there was concern that these values may have been tainted by suspect geostrophic velocities (Talley, 2003) and since the 11°S value differs significantly from nearly all other MHT estimates at this latitude, they were not included in the tables or figures.

Apart from these two particular values, throughout the South Atlantic, direct MHT estimates suggest northward transport with little gradient with latitude. Displaying remarkable consistency through data sets and methods, the weighted average of all the northward MHT estimates in Table 29.3 between 11 and 45°S that include estimates of uncertainty is 0.4 ± 0.2 PW. Note however, that the air–sea flux products disagree about the magnitude of the gradient in MHT in the South Atlantic (Figure 29.4). While the earlier NCEP1 and ERA-40 show little gradient, agreeing with the ECCO state estimation and direct observations, other and notably newer flux products show a fairly strong gradient in the South Atlantic. This disagreement is likely attributable to the regional biases mentioned in Section 2.1 and the fact that the older flux products contained specific flux corrections that are no longer used.

In summary, observation-based MHT estimates in the Atlantic reveal little gradient to the south of 15°S (about 0.4 PW); an increase to about 0.8 PW at 5°S; a cross-equatorial gradient that cannot be statistically distinguished from zero due to the large uncertainty arising from highly variable tropical winds and too few observations; and a maximum MHT of about 1.3 PW in the northern hemisphere subtropics (25°N), which decreases with increasing latitude (0.9 PW at 36°N, 0.6 PW at 47°N, 0.3 PW at 66°N). Issues affecting the estimates include technical details such as the low resolution of earlier sections and assimilative models, the choice of wind and air–sea flux products used as well as choices in how they are applied, and changes in the circulation itself, such as variable winds, seasonal changes in upper water column temperature, and differing MOC estimates.

3.2. Indo-Pacific

Like the Atlantic, the meridional transport of heat in the Pacific Ocean is principally poleward in the northern hemisphere. Recall that in the North Atlantic, the wind-driven gyre and the MOC are closely related and northward MHT arises from poleward transport of warm western boundary surface waters and southward return of waters that are on average colder and much deeper. In contrast, the Pacific wind-driven upper layer and deepwater overturning circulations exist in virtual isolation (Bryden et al., 1991; Wijffels et al., 1996). Pacific vertical overturn does not entail deepwater formation from ventilated surface waters but rather a deep overturning cell with a much smaller temperature difference between northward and southward components than in the Atlantic. The bulk of the northward MHT is a result of the wind-driven gyre circulation with poleward transport of warm surface waters and an only slightly cooler return flow within the thermocline (Bryden et al., 1991; Talley, 2003; Macdonald et al., 2009). Hence, in the North Pacific, poleward MHT occurs more as a result of the zonal relationship between temperature and velocity (wind-driven gyre) than the vertical relationship (overturn).

Reviewing the observations from north to south, at 47°N in the Pacific, none of the available estimates suggest any significant heat transport, but that is not to say that there are not significant north/south flows. Most of the strong flows appear to occur in the west where, according to Macdonald et al. (2009), the WBC carries 20.2×10^9 kg s^{-1} northward at a mean temperature of 3.7 °C (0.3 ± 0.1 PWT), which is compensated by a balancing return transport to the west of 160°E.

At 36°N, results are less conclusive as there is little consistency among the few available MHT estimates. Roemmich and McCallister (1989) suggest that their −0.16 PW is possibly underestimated due to poor sampling in the region of the WBC and note that a 10 Sv increase in Kuroshio transport at 15 °C would increase estimated MHT to +0.2 PW. If this is indeed the case, then the even greater southward estimate of Stammer et al. (2003) likely also suffers from the poor horizontal resolution of the underlying GCM. On the other hand, Wang and Carton's (2002) assimilation estimate using 2.5° horizontal resolution model finds a northward transport of ~0.35 PW, and the Talley (2003) estimate based on several cruises between 1965 and 1991, also northward, is twice as large again as this at 0.77 PW. This spread in estimates, that may have its origin in the spatial and temporal resolution of the observations and models used, is an indication that understanding the role Kuroshio plays in the region in both transporting energy northward and releasing it to the atmosphere is vital to our interpretation of the resulting estimates of MHT and its variability.

Though still presenting a fairly large range in possible values, MHT estimates near 24°N in the Pacific are more consistent than those at 36°N. This may be because the Kuroshio transport at this latitude is weaker, 24–33 Sv (Bingham and Talley, 1991; Ichikawa and Beardsley, 1993; Macdonald et al., 2009; Roemmich and McCallister, 1989) and more stable than to the north, 57–90 Sv (Book et al., 2002; Imawaki et al., 2001; Jayne et al., 2009; Macdonald et al., 2009). However, unlike 24°N in the Atlantic where a myriad of data sets are available, the mean Pacific MHT of 0.66 ± 0.28 PW comes from nine calculations, nearly all of which have been based on the same 1985 transect. The Uehara et al. (2008) estimate of 0.61 PW estimate stands out as it is based on XBT sections conducted between 1998 and 2002 between Honolulu and the east and west coast at ~22°N and 40°N, respectively.

The uncertainties in their calculation involved the estimated salinities and dearth of observations below the depth of the XBTs (about 800 m) and, as with all sections, sampling and Ekman transport estimation; the latter particularly because the section reaches as far south as 15°N in the tropics where the wind stress is more variable.

At 10°N, the weighted mean of the available estimates is 0.56 ± 0.86 PW with a spread of 1.2 PW. All these estimates are also surprisingly based on the same 1989 transect. It appears that the strong trade winds (capable of producing 25–40 Sv of Ekman transport across this latitude) and the strong currents that are known to be subject to both seasonal and interannual variations (Johnson et al., 2002) have made consistent estimation of a mean heat transport in the region difficult and highly susceptible to the details in choices of reference level, wind product, and so on.

Consideration of ocean heat or temperature transport closer to the equator is complicated by the highly variable, and therefore difficult to observe, flow through the Indonesian Archipelago (abbreviated as the Indonesian Throughflow or ITF; see Chapter 19). On a technical level, comparison of heat transport estimates is made more difficult because assumptions about where within the water column the compensation is expected to occur differ from study to study. Investigations within the Archipelago itself are further complicated by both geography and politics. The result is varying estimates such as the Indian Ocean hydrographic estimate of 1.4 PWT for a 15 Sv ITF (Ganachaud and Wunsch, 2000), a mooring estimate in the Makassar Strait of 0.55 PWT for a 10 Sv ITF (Vranes et al., 2002), Ekman transport estimates of ~0.5 PW for the southeast monsoon and ~1 PWT for the northwest monsoon timeframes (Sprintall and Liu, 2005), and a high-resolution modeling result of 1.1 PWT for 10.5 Sv (Pandey and Pandey, 2006).

In the South Pacific, the MHT is more properly called temperature transport because there is a net transport supporting the ITF. Because much of the water in the throughflow comes from the north, the temperature transport in the South Pacific is weak (see Table 29.4 references). Southern Indian Ocean temperature transports are strong (Figure 29.5), dominate the Indo-Pacific heat budget, and according to Vranes et al. (2002) lose negligible energy to the north of 30°S. The observational synthesis of Sultan et al. (2007) links southern Indian MHT intensity to the Agulhas Current strength and to the vertical mixing within the basin.

To summarize, the Indo-Pacific as a whole supports poleward heat transport in both hemispheres. There is little net meridional temperature transport in the South Pacific and strong southward temperature flux in the South Indian Ocean, supported partially by input from the North Pacific. As in the Atlantic, there is a maximum northern hemisphere MHT in the subtropics with lower values at higher latitudes. Many of the issues are the same as found in the Atlantic. In particular, more repeat observations are needed as strong, variable tropical winds present an even more serious problem to MHT estimates in the wide Pacific, while strong seasonality in the Indian Ocean requires more observations than presently available to gain better statistics.

3.3. Southern Ocean

In the Southern Ocean (SO), eddies play an increasingly important role in setting the MHT (Bryden, 1979; de Szoeke and Levine, 1981; Gille, 2003). Lagrangian float observations have determined an implied mean poleward eddy-driven MHT across the ACC of 0.3 ± 0.1 to 0.6 ± 0.1 PW. It is dominated by cross-stream fluxes in the Agulhas Retroflection region and supported by poleward fluxes in the ACC core (Gille, 2003). Satellite observations suggest that on decadal scales, SO wind-stress forcing is increasing (e.g., Dong et al., 2011; Thompson and Solomon, 2002). Increased winds contribute to both a stronger ACC and a richer eddy field. An eddy-resolving modeling study finds that such an increase first leads to a transient SO cooling due to increased northward Ekman transport, followed on longer timescales by a surface warming induced by the wind-enhanced eddy field (Hogg et al., 2008).

However, the SO is not solely dependent on eddies for MHT. Supported by an import of heat from the Brazil and Agulhas Currents, the ACC carries energy zonally from basin to basin within the Southern Ocean (Figure 29.5). Through its meridional excursions, it is warmed on its northward path in the Atlantic and Indian Basins and cooled on its way southward through the Pacific. In this way, the ACC directly contributes to the overall meridional energy budget with a mean baroclinic flow relative to 3000 dbar carrying -0.14 ± 0.01 PW, 0.095 ± 0.009 PW, and 0.082 ± 0.008 PW across 56°S, 58°S, and 60°S, respectively (Sun and Watts, 2002). Note that the flow below 3000 m is excluded from the Sun and Watts study. The ECCO2 synthesis of Volkov et al. (2010) concludes that transient features contribute to the gyre component, but not the overturning component. They show that the OHT in the SO is largely confined to the richly energetic fields of the Agulhas Retroflection and the Brazil-Malvinas Confluence. They also determine that the Indian Ocean sector is the dominant pathway for MHT due to the relatively large temperature contrast associated with this Warm Water Pathway of the MOC. The general northward MHT in the SO is opposed by deep AABW overturn. An OCCAM high-resolution model designed to better resolve AABW export finds that although transients contribute to the MHT, deep overturn is responsible in the annual mean for a southward MHT of -0.033 PW, and on shorter timescales for as much as -0.061 PW (Heywood and Stevens, 2007).

In summary, there are few hydrographically based estimates of MHT in the SO. This lack is due partially to the difficulty of the calculation in a region with minimal boundaries, where so many isopycnals outcrop and winds are so strong. It is also due to a severe lack of data. SO observations are notoriously difficult to obtain and hard to analyze. For this reason, much of what is known comes from other sources such as remote instrumentation (e.g., floats and satellites) and models. With strong variability and strong surface fluxes, the SO exemplifies the need to understand the interaction between the ocean and the atmosphere to better interpret OHT estimates and to predict seasonal and climate-scale changes.

4. UNDERSTANDING MECHANISMS

As described in Section 3, there is a large and growing database of observations that can provide MHT and OHT values to be compared and used to improve our understanding of how the ocean moves energy from one location to another. A variety of techniques have been developed to investigate the physical mechanisms of these energy transfers. In particular, to better understand how the underlying ocean circulation transports energy (i.e., heat) from one place to another, a number of different decomposition techniques have been employed. Here we describe two such methods.

4.1. Barotropic-Baroclinic-Horizontal Decomposition (BBH)

Hall and Bryden (1982) decomposed MHT in their analysis at 25°N in the Atlantic into a depth-averaged transport (barotropic) and a depth dependent transport (baroclinic). Bryan (1962), in his analysis of model results, suggested a similar decomposition that included a third, smaller term representing horizontal diffusion. Recognizing the unique contribution of both horizontal and vertical overturn to ocean MHT, Bryden and Imawaki (2001) put forth a variation on the barotropic/baroclinic (BB) decomposition. Reminiscent of the Bryan (1962) method, this decomposition more directly discriminates between the two components. It separates the velocity and temperature terms in Equation (29.1) into a barotropic component based on the section averaged velocity $[v]$, temperature $[\Theta]$ and density $[\rho]$:

$$[\rho]\,[\mathrm{Cp}]\,[v]\,[\Theta]\iint \mathrm{d}x\mathrm{d}z,$$

a baroclinic component based on the horizontal average values $\langle v\rangle(z)$ and $\langle\Theta\rangle(z)$:

$$\int \rho\mathrm{Cp}\langle v\rangle(z)\,\langle\Theta\rangle(z)\int \mathrm{d}x\mathrm{d}z,$$

and a horizontal (gyre) component based on the horizontal anomalies: $v'(x, z)$ and $\Theta'(x, z)$

$$\int \mathrm{d}z\int \rho\mathrm{Cp}v'(x,z)\,\Theta'(x,z)\mathrm{d}x,$$

where, $v=[v]+\langle v\rangle(z)+v'(x,z)$ and $\Theta=[\Theta]+\langle\Theta\rangle(z)+\Theta'(x,z)$. We refer to this technique as the BBH—barotropic, baroclinic, and horizontal decomposition.

In their investigation comparing the 2009 and 1983 meridional heat and freshwater transports across 24°S in the Atlantic, Bryden et al. (2011) used this decomposition to illustrate the strong heat transport associated with overturning circulation (0.76 PW in 2009 and 0.53 PW in 1983) and the weaker (−0.07 PW in 2009 and −0.14 PW in 1983) horizontal component dominated by the shallow southward flowing western boundary Brazil Current. The removal of the section-average barotropic term in this decomposition forces a zero net mass transport for both the baroclinic and the horizontal terms. This allows for a comparison of these terms even when a net mass transport is unavoidable as is the case for the ACC, Pacific-Indian Throughflow, and indeed any zonal transect affected by Bering Strait throughflow and/or freshwater transport. The utility of intercomparing different sections using this decomposition was shown by Lavín et al.'s (2003) analysis of hydrographic lines spanning three decades. Here, rather than using an estimate of the absolute velocity field, they simplified their analysis by combining the wind-driven component with the barotropic term, thus making the other two terms more easily comparable.

4.2. Shallow Subducting Overturn Decomposition (SOV)

A different decomposition technique (Roemmich and Wunsch, 1985) has been applied globally by Talley (2003) to separate the heat transport associated with the shallow, subducting component of subtropical gyres from that accompanying deep meridional overturn. This decomposition is based on the premise that whether or not deep overturn exists or is dominant, shallow gyre overturn will occur in the presence of a warm poleward-oriented WBC, whose waters are cooled along its path and subducted (i.e., overturned) before returning equatorward. This process is typical of wind-driven gyres subject to air–sea buoyancy loss and should be distinguished from intergyre/interhemispheric large-scale overturn. As mentioned earlier, this shallow subducting overturn (SOV) dominates in the Pacific (Bryden et al., 1991). Talley (2003) hypothesizes that it is present to a greater or lesser degree in all subtropical gyres, and the goal of the decomposition is to estimate the relative influence of intermediate, deep, and bottom flows on the MHT.

The technique which is referred to here as the SOV method is outlined as follows: (a) The base of the SOV is defined as the maximum wintertime density along the zero-Sverdrup transport line between the subtropical and

subpolar gyres. This definition is chosen to separate the shallow heat transport arising from cooling of the near-surface wind-driven gyre circulation from that supported by deeper overturn as it represents the densest water that could be subducted within the gyre. The density and depth of the SOV vary considerably from basin to basin. For example (Talley, 2003), the SOV base taken as $\sigma_\theta = 27.3$ lies between ~700 and 800 m at 24°N in the Atlantic compared to the $\sigma_\theta = 26.2$ SOV base lying between ~100 and 600 m at the same latitude in the Pacific; (b) Above the SOV base, along a transect within the subtropical gyre, interior geostrophic transports are summed with the Ekman transport perpendicular to the section and that portion of the WBC transport that provides either mass balance or a known net mass transport. Talley suggests two methods of distributing the WBC portion to yield upper and lower estimates of poleward heat transport. Net transports across the sections are also apportioned so as to provide extrema for the estimated heat transport values; (c) The estimated SOV mass transports are subtracted from the total transports in the SOV layers to provide an estimate of the transport that is assumed to be transformed into water denser than that associated with the SOV, and here Talley assumes that this water is transformed into the nearest available density class; (d) Then, heat and temperature transports are calculated by zonal integration within density classes.

Although subjective in nature, with judicious selection of extrema, the SOV technique provides a unique view into the circulation of energy within the ocean. It improves understanding and quantification of the water mass transformations associated with the subduction process, which otherwise have a tendency to be lumped into a single "horizontal" or "gyre," nonoverturn value. Using this technique, Talley (2003) found that there is a measureable SOV within each of the subtropical gyres. This SOV water is transformed into an intermediate density class (500–2000 m) in the northern-hemisphere gyres, or into deep density classes in the southern-hemisphere gyres and that portion of the North Atlantic influenced by deep overflows. Further, she determined that separated from the SOV, Indo-Pacific temperature transport associated with ITF is modest (≤0.1 PWT) and the bulk of the Indo-Pacific MHT is carried in the shallow "supergyre" overturn that includes the ITF. Formation rates of NADW and AABW are similar. However, because temperature differences between NADW/LCDW and AABW at 30°S are relatively small, the heat transport associated with Antarctic dense water formation is similarly small.

In summary, both the BBH and SOV techniques look to separate the throughflow, overturning, and horizontal transports. According to all the decomposition methods, deep overturn is the dominant mechanism by which heat is transported northward (88% according to Johns et al. (2011) BB method; 67% Talley (2003) SOV method; 62% Lavin et al. (2003) BBH method) in the subtropical North Atlantic. Nevertheless, by most accounts, the horizontal/gyre component is nontrivial unless, as Talley (2003) points out, the warm WBC water is not strongly surface-intensified. If this is the case, the portion of the total heat transport for which the SOV is responsible is reduced due to a reduction in temperature contrast between the WBC and the subtropical gyre return flow. In the North Pacific, all studies find that MHT is dominated by shallow gyre scale overturn (Table 29.2, Figure 29.5). However, Talley (2003) concluded that due to differing underlying assumptions, the BBH and SOV decompositions are not directly comparable. Regardless of the decomposition used, the user must still make choices regarding the Ekman component, which wind product to use, and how to apply it. Neither method includes a time varying component although there is no mathematical reason why they should not. Variability within the ocean has been recognized for a long time, but acquiring the necessary observations for estimating variations in OHT has only recently been initiated.

5. OCEAN HEAT TRANSPORT VARIABILITY

Ocean heat transport variability estimates have been derived from observations using several techniques, including repeat full water column hydrography (providing exceptional spatial resolution and extremely poor temporal resolution); *in situ* partial water column (surface to 750 or 2000 m) XBT and Argo data (providing better temporal resolution and for the latter, improved spatial coverage); and moored instruments spanning the breadth of a basin providing a spatially subsampled data set with excellent temporal resolution. Global ocean general circulation model and coupled model assimilations (see Chapters 21 and 22) provide a means to combine multiple and varied observations and generate time series linking the more sparse observations. The expectation is that model results will better represent reality when they are consistent with observations, and interpretation of diverse observations will be improved by imposing conservation equations. Originally including satellite altimetry, historical hydrography, and atmospheric estimates of surface forcing (Carton et al., 2000a,b; Stammer et al., 2002), they now assimilate most of the types of available water column observations (e.g., repeat hydrography, profiling float, expendable bathythermograph (XBT) and mooring time series data, etc.) as constraints on temporally varying state estimates of ocean circulation (Davis et al., 2011; Heimbach et al., 2011; Wunsch and Heimbach, 2009).

The discussion here focuses on observations in the Atlantic, and in particular, at 24–27°N because this is where most time series observations are presently available and the most research has been done. Results from other basins are provided where they are available. We include discussion

of historical hydrography because, although not ideal as a time series, at most locations these are the only data available for temporal comparison of full water column MOC/MHT.

5.1. Repeat Hydrography

Initial variability estimates based on repeat hydrography along 48°N in the Atlantic suggest conflicting conclusions relative to the state of the thermohaline circulation and MHT. In particular, Koltermann et al. (1999) conclude that the strong MOC/MHT variability they saw was related to the strength of Labrador Sea Water (LSW) production, with larger (smaller) MOC/MHT corresponding to less (more) LSW export. The same data (1993–2000), reanalyzed to formally test whether MOC circulation is steady, concluded that a steady MOC could not be ruled out due to the uncertainty in determining the barotropic circulation, and the observed range in MHT variability (0.51–0.55 PW) could not be characterized as a trend (Lumpkin et al., 2008).

A similar full analysis, at 24°N in the subtropical Atlantic, concluded that the thermohaline circulation had declined over the previous 50 years by 30% (Bryden et al., 2005), a much higher rate of change than predicted in coupled climate model simulations (e.g., Schmittner et al., 2005). A comparable study using 24°N hydrography collected through 1998 showed similar MOC variability, but no decadal-scale trend in MHT could be verified due to strong seasonal variability (Baringer and Molinari, 1999). As more complete time series became available, these differences between hydrographic estimates were recognized as aliased seasonal and interannual variations (see Section 5.2). Hernández-Guerra et al. (2009) used Argo float data to reduce the eddy signal seen in the 24–26°N repeat hydrographic sections and showed that no significant change in MOC had occurred since the earliest 1957 transect. Longworth et al. (2011) examined 26°N MOC variability using a database of end-point measurements from the past 50 years. This improvement to the Bryden et al. (2005) statistics verified that no significant trend in the MOC had been observed. Nevertheless, the indirectly estimated NCEP record does suggest some longer time-scale trends both in MHT and the latitude of the MHT (Figure 29.6).

5.2. Transition to Timeseries Arrays

Since 1982, variations in the upper limb of the MOC at 27°N have been monitored by measuring the Florida Current transport using a submarine cable across the Straits of Florida in combination with repeat hydrography (Baringer and Larsen, 2001; Meinen et al., 2010). In 1984, monitoring was expanded to the deep limb of the MOC through regular hydrographic cruises (more than 30 to date) across the DWBC east of the Bahamas (van Sebille et al., 2011), and in 2001 the program commenced time series monitoring of the DWBC by adding moored inverted echo sounders and bottom pressure gauges east of Abaco Island in the Bahamas (Meinen et al., 2006). In 2004, the effort was substantially enhanced and became international, expanding the MOC monitoring array to span

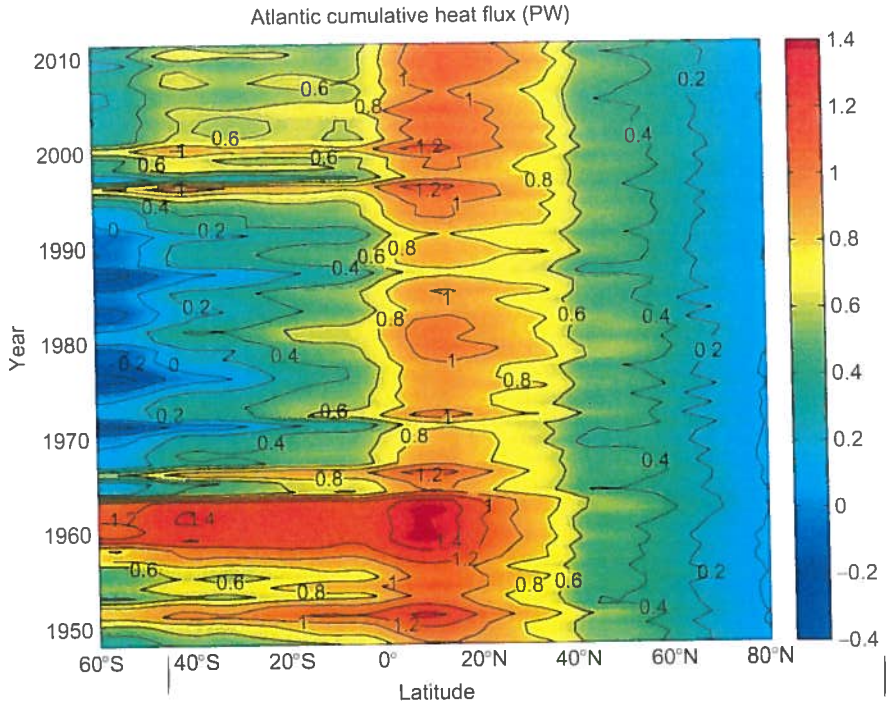

FIGURE 29.6 Illustration of annual to decadal variability. NCEP CORE-v2 estimates of meridional heat transport in the Atlantic integrated from north to south.

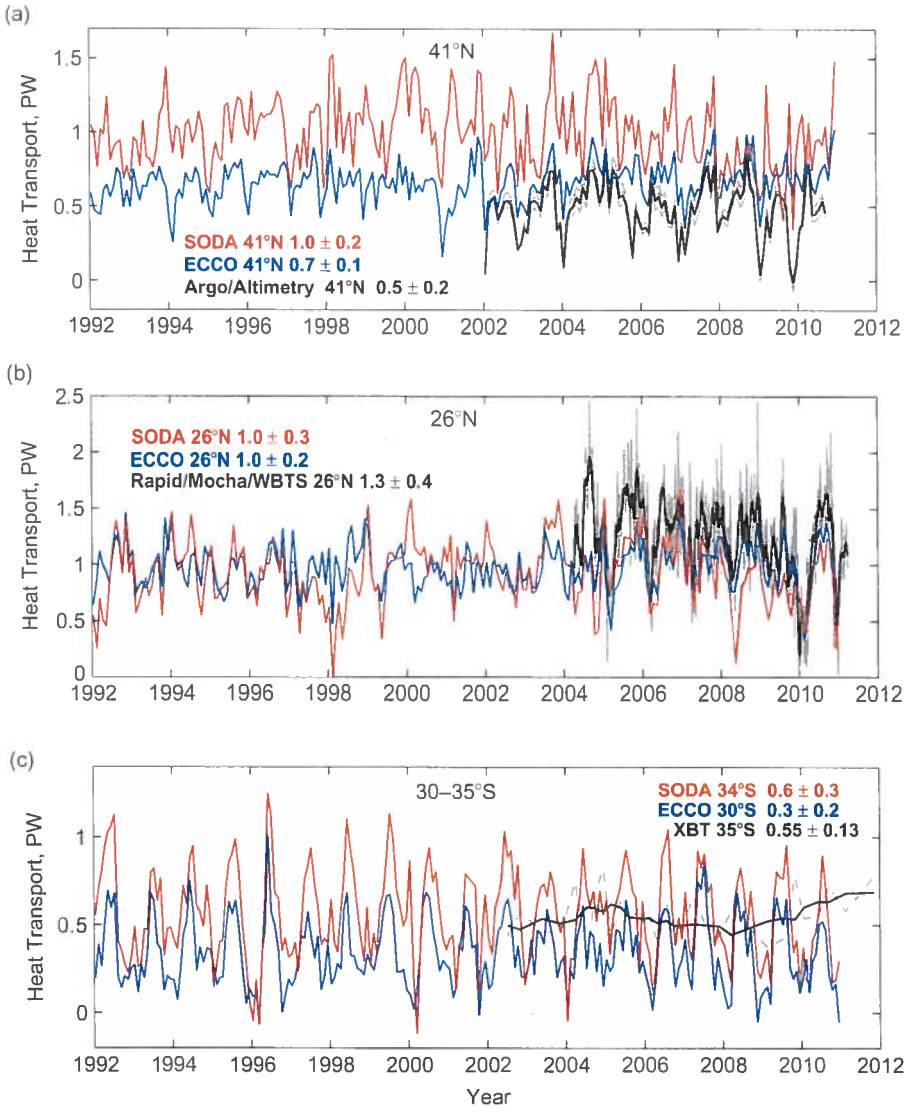

FIGURE 29.7 Assimilation timeseries of Atlantic MHT from SODA V2.2.4 (Giese and Ray, 2011) and ECCO-PROD version 4 (Wunsch and Heimbach, 2013) compared to: (a) the profiling float time series (Hobbs and Willis, 2012) at 41°N; (b) the RAPID/MOCHA mooring/hydrography time series (Johns et al., 2011) at 26°N; and (c) the repeat XBT ship-of-opportunity time series at ~30°S (updated from Garzoli et al., 2012). Values in the legends indicate means and standard deviations over the illustrated time periods. Please note the limits of the vertical axes in the panels are different (units in PW), positive is northward.

the entire Atlantic Basin at 26°N using a variety of measurement systems (Rayner et al., 2011). Called the RAPID Climate Change Program by the UK contributors and the Meridional Overturning Circulation Heat-Transport Array (MOCHA) by the US contributors, this expanded project seeks to develop a cost-effective basin-wide MOC monitoring system that will lead to a much greater degree of certainty in the magnitude of the variations in the integrated, basin-wide MOC and the time scales of variation (Kanzow et al., 2007, 2008).

The results from this array quickly indicated significant variability in all components of the MOC, and the entire range of MOC values suggested by the repeat hydrography was encountered within the first year of the time series (Figure 29.7b; Cunningham et al., 2007). The time series continues to indicate strong variability at a range of time scales, including the emergence of an annual cycle (Kanzow et al., 2010) that looks similar to the annual cycle postulated on the basis of the repeat hydrography at 24°N (Baringer and Molinari, 1999). Of note is that all the upper ocean transport values estimated by Bryden et al. (2005) from five repeat CTD sections can be found within the seasonal range of the interior transport time series (Baringer et al., 2009; Kanzow et al., 2010). This array is now providing an unprecedented continuous time series of MHT in the subtropical North Atlantic (Johns et al., 2011).

Results have provided unique quantification of the seasonal amplitude in heat transport (0.6 PW annual range), confirmation of the large variability found at short time scales (MHT values ranging from 0.2 to 2.5 PW), and a change in our understanding about what controls the variability in MHT versus the mean MHT. As noted earlier, the mean MHT in the subtropical North Atlantic is largely determined by the mean overturn strength (carrying 88% of the total MHT). Based on 3.5 years of data, the Ekman layer is responsible for 50% of the variance in MHT, while it is only responsible for a small portion of the mean MHT.

5.3. Float Program

The Argo float program has provided upper water column temperature measurements throughout the global ocean for nearly a decade. With approximately 3800 floats presently in the water, Argo is producing 100,000–135,000 profiles each year (P.E. Robbins, personal communication, 2013) in a data set that improves our global coverage with unprecedented spatial resolution and little seasonal bias. These profiles can be combined with velocity estimates and assumptions about the circulation below 2000 m to estimate, among other things, heat transport. Time-varying estimates of Argo-based Atlantic MHT suggest a 7-year mean at 41°N of 0.50 ± 0.1 PW with strong seasonal variability (Figure 29.7a, Hobbs and Willis, 2012). Strong, seasonal variability is a characteristic of the Atlantic ECCO solution (Figure 29.7) as well as indirect and model estimates (see Chapter 24). The latter can, with a longer time-series, see evidence of MHT variability on longer timescales even away from the tropics (Figure 29.6 and see Chapter 25). As RAPID/MOCHA concluded at 24°N, Hobbs and Willis (2012) reported, based on the float record, a nonsignificant decreasing trend of -0.05 PW decade^{-1}.

Hobbs and Willis (2012) consider their uncertainty estimate to be a lower limit because it does not include decadal-scale variability. Going to longer time-scales requires the use of models. Zheng and Giese (2009) found a positive trend of 0.036 PW decade^{-1} significant at >95% at 40°N using data assimilation over a 50-year period. In fact, all the significant trends they reported for the Atlantic suggested an increase in northward heat transport, which they believe is associated with an increasing trend in mid-latitude overturn. This strengthening of the overturn appears to be related to the northward shift of the atmospheric circulation discussed in the AR4 Report.

5.4. Ships of Opportunity and Expendable Instrumentation

Volunteer ships of opportunity and expendable instrumentation have allowed repeat measurements of upper ocean hydrography along specific shipping lanes. Note that in the following discussion estimates are calculated for flow across these lanes, which are not always directly comparable to the basin transects occupied by research vessels. Roemmich et al. (2001) used high-resolution XBT data and XCTD observations to determine MHT variability from 1992 to 1999 in the North Pacific, where the upper layers that carry most of the heat transport (Bryden et al., 1991) are also subject to strong temporal variability. Using the repeat transects (~four 17-day, 10 km resolution sections between 15 and 35°N each year over the period of the study), they found a mean 0.83 ± 0.12 PW, slightly higher relative to other midlatitude estimates (Table 29.4) with the variability in Ekman transport (northward) balanced by variability in the interior transport (southward). The interannual variability O(0.4 PW) represents a substantial fraction of their estimated mean and appears to correspond to variation in the North Pacific Index. Roemmich et al. also showed that interannual variability in eddy heat fluxes can be quite large O(0.15 PW) and concluded that closure of the net heat budget was attainable with improved MHT time series estimates, air–sea flux products, and ocean heat storage estimates.

The South Atlantic has been historically one of the least sampled basins. As a consequence, model estimates in this region have been relatively unconstrained. In the past decade, however, the picture has been changed by multiple, high-density XBT lines (AX18 at 35°S from Brazil to South Africa, AX22 across Drake Passage, and AX25 across the Agulhas retroflection; Garzoli and Baringer, 2007; Stephenson et al., 2012; Swart et al., 2008), and broad scale temperature and salinity profiles collected by the Argo program (Roemmich and Owens, 2000). AX18 observations from 2002 onward have been used to study MOC variability and its effect on the net northward South Atlantic MHT (Garzoli et al., 2012). This analysis shows that the South Atlantic is responsible for a (2002–2011) mean northward MHT of 0.55 ± 0.13 PW (slightly higher than section estimates, Table 29.3), and in agreement with the 50-year SODA assimilation (Zheng and Giese, 2009) with no significant trend (Figure 29.7c; Dong et al., 2011). Although geostrophic transport dominates the time-mean MOC/MHT, both the geostrophic and Ekman components are important in explaining the variability as they display out of phase annual cycles that result in weak seasonal variability (Baringer and Garzoli, 2007; Dong et al., 2009). Examination of the contributions from boundary currents and the interior indicates that transport variability of all three regions is comparable. MHT variability is significantly correlated with the MOC variability, where a 1 Sv increase in the strength of MOC would yield a 0.05 ± 0.01 PW increase in the MHT. Thus a 5–6% MOC change results in a 10% change in the MHT, clearly illustrating the climatic importance of accurately monitoring the MOC.

Until recently, models have suggested a strong annual cycle for the total MHT and MOC in the South Atlantic that depends mainly on the seasonal cycle of the Ekman component and very little on the geostrophic component of the fluxes (Böning et al., 2001; Dong et al., 2009; Jayne and Marotzke, 2001). Now, new results suggest that climate models may be underestimating oceanic geostrophic variability (e.g., Sarojini et al., 2011).

5.5. Summary of Observational Approaches

A variety of measurement and analysis techniques are currently being used to better understand heat transport variability on differing temporal scales. Hydrography is presently the only method available for obtaining full water-column land-to-land observations at multiple latitudes. Repeat transects have suggested signals (e.g., annual cycle) that more complete time series have measured or could measure, but seasonal variability reduces its effectiveness as a means for determining temporal trends in transport. Use of ships of opportunity and expendable instruments has allowed improved temporal and spatial coverage at some cost to choice of path and vertical coverage, while the now prodigious profiling float record allows for greater horizontal coverage.

The RAPID/MOCHA array in the subtropical North Atlantic is providing an enviably complete OHT time series at a single latitude and has been improved over time to include bottom and mid-ocean measurements. This time series continues to indicate strong variability at a range of time scales, including the emergence of a possible annual cycle and substantial short-term variability such as the abrupt weakening of the MOC in the winter of 2009–2010 (McCarthy et al., 2012). Given another 5 years of observations, examination of interannual cycles should be feasible (Cunningham et al., 2007). Nevertheless, it is unlikely that this type of array can provide the large-scale latitudinal coverage that is needed. In some regions, time-series that focus on particular aspects of the circulation (e.g., WBC or shallow overturn) are necessary for improved statistics. For other regions, continued repeat hydrography, VOS/XBT, float programs, and improved data assimilating models represent our best opportunities for obtaining the spatial and temporal coverage necessary for observing changes in OHT, as well as long-term trends in temperature and salinity that could directly or indirectly affect OHT.

6. SYNTHESIS AND SUMMARY

Transport of heat by the oceans is one of the dynamic components of the earth's energy budget. In providing a brief background on the global energy balance, we have touched upon the similarities and differences in the roles played by the atmosphere (an efficient homogenizer) and ocean (the long term memory) in maintaining the balance, as well as the importance of the interactions between them. There are spatial asymmetries in the energy budget resulting from the earth's orientation to the sun and the spatial variation in absorbed radiation. These asymmetries support a transfer of energy from the tropics toward the poles. Observational and model estimates of maximum total poleward heat transport are consistent and range between 5.3 and 5.9 PW depending upon hemisphere and method of calculation. As at the top of the atmosphere, incoming shortwave solar radiation at the surface of the ocean supplies stronger warming at the equator than at the poles. However, there are spatial variations in the loss of heat by the ocean through sensible and latent heat fluxes, as well as differences in ocean basin geometry and current systems. These complexities support a pattern of ocean heat transport that is not strictly from lower to higher latitudes.

Three methods for calculating OHT have been discussed. Two of these, the bulk formula method and the residual method, are considered "indirect" as they do not require observations of the ocean. The advantage of these estimation techniques is that they can provide complete global coverage and long, high-resolution timeseries OHT estimates. They also directly connect OHT to atmospheric processes through air–sea interactions. They afford an excellent basis from which to investigate variations in OHT on seasonal and longer time-scales, as well as feedbacks and changes in feedbacks that could result in changes in OHT. Their disadvantage is that they tend to contain strong regional biases that are likely due to missing or inadequately represented physics and spatial inhomogeneity of the underlying data (in both amount and type of data) that cannot be easily removed. The third method for calculating OHT is considered "direct" because it is based on observations of ocean properties. This technique, which requires estimates of ocean temperature, salinity, and velocity fields, was originally used with long-line hydrography, but is now being used with float profiles, data from volunteer ship of opportunity expendable instrumentation, trans-basin time series mooring-array data, and altimetry.

On average, MHT estimates support a global poleward heat flux in the Atlantic and Indo-Pacific with maxima in the subtropics. The mean maximum global MHT from the values presented here is 1.6 ± 0.4 PW at 24°N (slightly less than 1/3 of total). In the Atlantic, the maximum lies in the northern hemisphere and is sustained by meridional overturn. In the Indo-Pacific, the southern hemisphere MHT maximum dominates. Supported mainly by Indian Ocean outflow, it represents a temperature flux maintained by the warm ITF. Mean estimates of South Atlantic and North Pacific subtropical MHT maxima are about half the magnitude of their counterparts (in the North Atlantic and southern Indo-Pacific, respectively) and are associated with strong gyre components of the circulation.

Although uncertainties are greatest in the tropics mainly due to strong, variable winds, there remains a relatively large range in estimates in the subtropical North Pacific. Although not presented, the same is true in the South Pacific. The range appears to be largely due to how shallow overturn is represented, as shallower overturn produces smaller MHTs. The XBT record has also pointed to a strong MHT/MOC connection in the South Atlantic.

Uncertainties in OHT estimates have been attributed to insufficient spatial resolution of both observations and models that lead to uncertainties in WBC and MOC mass transports. OHT estimates are also affected by strong unresolved seasonal signals in the winds and circulation. Some specific challenges for the future include clarifying the effects of WBC variability (e.g., Garzoli and Matano, 2011); the role of eddies, particularly in the South Atlantic (e.g., Biastoch et al., 2008; Duncombe Rae et al., 1996) and Southern Ocean (e.g., Gille, 2003) where their effects need to be separated from changes in wind-forcing (Meredith et al., 2012); the effect of ITF variability (e.g., Corell et al., 2009); the influence of strong seasonal changes circulation and in the magnitude of the southern deep inflow in the Indian Ocean (Schott et al., 2009; Sultan et al., 2007).

To improve statistics in these regions, as well as in the observation-poor Southern Ocean, more complete or longer *in situ* time series are necessary. Such observations can be used on their own or to confirm and/or constrain model estimates and predictions. At present, observing systems capable of quantifying changes in MHT are at fledgling stages. At 26.5°N in the Atlantic, the RAPID/MOCHA program (Johns et al., 2011; Kanzow et al., 2008) has for the first time provided the elements of a continuous time-series of meridional overturn and its associated heat transport across a latitude line. However, such data sets need not necessarily be always cross-basin and full-depth. For instance, in the North and South Pacific, observations that provide a clearer picture of the depth, magnitude, and variability in shallow overturn would go a long way toward improving our understanding of Pacific OHT. In the Indian Ocean, observations that focus on deep overturn, mixing, and seasonal changes would likewise benefit our interpretation of OHT estimates. And in the Atlantic, observations such as the MOVE array monitoring the deep circulation (Send et al., 2011) and the float time series (Willis, 2010) will become increasingly valuable as we seek to understand the meridional coherence of MOC and MHT fluctuations. Throughout the global ocean, the long-transect hydrographic survey that began as WOCE in the 1990s and was extended as CLIVAR in the 2000s, now continues into the new century as GO-SHIP. Still temporally sparse, at present it provides the only high-quality, global, full-depth, cross-basin timeseries available for studying OHT.

REFERENCES

Abbot, C.G., Fowle, F.E., 1908. Determination of the intensity of the solar radiation outside the earth's atmosphere, otherwise termed "the Solar Constantant of Radiation" Annals of Astrophysical Observatory of the Smithonsian Institution. 2(1). Smithsonian Institution, Washington, DC, pp. 1–237.

Bacon, S., 1997. Circulation and fluxes in the North Atlantic between Greenland and Ireland. J. Phys. Oceanogr. 27, 1420–1435.

Baringer, M.O., Molinari, R., 1999. Atlantic Ocean baroclinic heat flux at 24° to 26°N. Geophys. Res. Lett. 26, 353–356.

Baringer, M.O., Larsen, J., 2001. Sixteen years of Florida Current transport at 27 N. Geophys. Res. Lett. 28 (16), 3179–3182.

Baringer, M.O., Garzoli, S.L., 2007. Meridional heat transport determined with expendable bathythermographs, Part I: error estimates from model and hydrographic data. Deep Sea Res. Part I 54 (8), 1390–1401.

Baringer, M.O., Meinen, C.S., Johnson, G.C., Kanzow, T.O., Cunningham, S.A., Johns, W.E., Beal, L.M., Hirschi, J.J.-M., Rayner, D., Longworth, H.R., Bryden, H.L., Marotzke, J., 2009. The meridional overturning circulation. In: Peterson, T.C., Baringer, M.O. (Eds.), State of the Climate in 2008, Bulletin of the American Meteorological Society, vol. 90(8), pp. S59–S62.

Beal, L.M., Chereskin, T.K., Bryden, H., Ffield, A., 2003. Variability of water properties, heat and salt fluxes in the Arabian Sea, between the onset and wane of the 1995 southwest monsoon. Deep Sea Res. Part II 50, 2049–2075.

Beal, L.M., De Ruijter, W.P.M., Biastoch, A., Zahn, R., SCOR/WCRP/IAPSO Working Group 136, 2011. On the role of the Agulhas system in ocean circulation and climate. Nature 472, 429–436.

Berry, D.I., Kent, E.C., 2009. A new air–sea interaction dataset from ICOADS with uncertainty estimates. Bull. Am. Meteorol. Soc. 90 (5), 645–656.

Biastoch, A., Böning, C.W., Lutjeharms, J.R.E., 2008. Agulhas leakage dynamics affects decadal variability in the Atlantic overturning circulation. Nature 456, 489–492.

Bingham, F.M., Talley, L.D., 1991. Estimates of Kuroshio transport using an inverse technique. Deep Sea Res. 38 (Suppl. 1A), 21–43.

Böning, C.W., Dieterich, C., Barnier, B., Jia, Y., 2001. Seasonal cycle of meridional heat transport in the subtropical North Atlantic: a model intercomparison in relation to observations near 25°N. Prog. Oceanogr. 48, 231–253.

Book, J.A., Wimbush, M., Imawaki, S., Ichikawa, H., Uchida, H., Kinoshita, H., 2002. Kuroshio temporal and spatial variations south of Japan determined from inverted echo sounder measurements. J. Geophys. Res. 107 (C9), 3121. http://dx.doi.org/10.1029/2001JC000795.

Bosilovich, M.G., Robertson, F.R., Chen, J., 2011. Global energy and water budgets in MERRA. J. Clim. 24, 5721–5739.

Bourras, D., 2006. Comparison of five satellite-derived latent heat flux products to moored buoy data. J. Clim. 19, 6291–6313.

Brodeau, L., Barnier, B., Treguier, A.-M., Penduff, T., Gulev, S., 2010. An ERA40-based atmospheric forcing for global ocean circulation models. Ocean Model. 31, 88–104.

Bromwich, D.H., Wang, S.-H., 2005. Evaluation of the NCEP–NCAR and ECMWF 15- and 40-Yr reanalyses using Rawinsonde Data from two independent arctic field experiments. Mon. Weather Rev. Special Section 133, 3562–3577.

Bryan, K., 1962. Measurements of meridional heat transport by currents. J. Geophys. Res. 67 (9), 3403–3414.

Bryden, H.L., 1979. Poleward heat flux and conversion of available potential energy in Drake Passage. J. Mar. Res. 37, 1–22.

Bryden, H.L., Imawaki, S., 2001. Ocean heat transport. In: Siedler, G., Church, J., Gould, J. (Eds.), Ocean Circulation and Climate. Academic Press, London, pp. 455–474. Chapter 6.2.

Bryden, H.L., King, B.A., McCarthy, G.D., 2011. South Atlantic overturning circulation at 24° S. J. Mar. Res. 69 (1), 38–55.

Bryden, H.L., Longworth, R., Cunningham, S., 2005. Slowing of the Atlantic meridional overturning circulation at 25° N. Nature 438, 655–657.

Bryden, H.L., Roemmich, D.H., Church, J.A., 1991. Ocean heat transport across 24° N in the Pacific. Deep Sea Res. 38, 297–324.

Carton, J.A., Chepurin, G., Cao, X., Giese, B.S., 2000a. A Simple Ocean Data Assimilation analysis of the global upper ocean 1950–1995, Part 1: methodology. J. Phys. Oceanogr. 30, 294–309.

Carton, J.A., Chepurin, G., Cao, X., 2000b. A Simple Ocean Data Assimilation analysis of the global upper ocean 1950–1995 Part 2: results. J. Phys. Oceanogr. 30, 311–326.

Carton, J.A., Giese, B.S., 2008. A reanalysis of ocean climate using Simple Ocean Data Assimilation (SODA). Mon. Weather Rev. 136, 2999–3017.

Compo, G.P., Whitaker, J.S., Sardeshmukh, P.D., Matsui, N., Allan, R.J., Yin, X., Gleason, B.E., Vose, R.S., Rutledge, G., Bessemoulin, P., Brönnimann, S., Brunet, M., Crouthamel, R.I., Grant, A.N., Groisman, P.Y., Jones, P.D., Kruk, M., Kruger, A.C., Marshall, G.J., Maugeri, M., Mok, H.Y., Nordli, O., Ross, T.F., Trigo, R.M., Wang, X.L., Woodruff, S.D., Worley, S.J., 2011. The Twentieth Century Reanalysis Project. Q. J. R. Meteorol. Soc. 137, 1–28. http://dx.doi.org/10.1002/qj.776.

Corell, H., Nilsson, J., Döös, K., Broström, G., 2009. Wind sensitivity of the inter-ocean heat exchange. Tellus 61A, 635–653.

Cunningham, S.A., Kanzow, T., Rayner, D., Baringer, M.O., Johns, W.E., Marotzke, J., Longworth, H.R., Grant, E.M., Hirschi, J.J.-M., Beal, L.M., Meinen, C.S., Bryden, H.L., 2007. Temporal variability of the Atlantic meridional overturning circulation at 26.5° N. Science 312, 335–938. http://dx.doi.org/10.1126/science.1141304.

da Silva, A., Young, A.C., Levitus, S., 1994. Atlas of surface marine data 1994. Technical Report 6, vol. 1 U.S. Department of Commerce, NOAA, NESDIS, 83 pp.

Davis, X.J., Rothstein, L.M., Dewar, W.K., Menemenlist, D., 2011. Numerical investigations of seasonal and interannual variability of North Pacific. J. Clim. 24, 2648–2665.

Dee, D., Uppala, S.M., Simmons, A.J., Berrisford, P., Poli, P., Kobayashi, S., Andrae, U., Balmaseda, M.A., Balsamo, G., Bauer, P., Bechtold, P., Beljaars, A.C.M., van de Berg, L., Bidlot, J., Bormann, N., Delsol, C., Dragani, R., Fuentes, M., Geer, A.J., Haimberger, L., Healy, S.B., Hersbach, H., Hólm, E.V., Isaksen, L., Kållberg, P., Köhler, M., Matricardi, M., McNally, A.P., Monge-Sanz, B.M., Morcrette, J.-J., Park, B.-K., Peubey, C., de Rosnay, P., Tavolato, C., Thépaut, J.-N., Vitart, F., 2011. The ERA-Interim reanalysis: configuration and performance of the data assimilation system. Q. J. R. Meteorol. Soc. 137, 553–597.

de Szoeke, R.A., Levine, M.D., 1981. The advective flux of heat by mean geostrophic motions in the Southern Ocean. Deep Sea Res. Part A 28, 1057–1085.

Dines, W.H., 1917. The heat balance of the atmosphere. J. R. Meteorol. Soc. 43, 151–158.

Dong, S., Garzoli, S., Baringer, M., 2011. The role of interocean exchanges on decadal variations of the meridional transport of heat in the South Atlantic. J. Phys. Oceanogr. 41, 1498–1511.

Dong, S., Garzoli, S., Baringer, M., Meinen, C., Goni, G., 2009. Interannual variations in the Atlantic meridional overturning circulation and its relationship with the net northward heat transport in the South Atlantic. Geophys. Res. Lett. 36. http://dx.doi.org/10.1029/2009GL039356, L20606.

Donohoe, A., Battisti, D.S., 2012. What determines meridional heat transport in climate models? J. Clim. 25, 3832–3850. http://dx.doi.org/10.1175/JCLI-D-11-00257.1.

Douglass, E., Roemmich, D., Stammer, D., 2010. Interannual variability in North Pacific heat and freshwater budgets. Deep Sea Res. Part II 57 (13–14), 1127–1140.

Duncombe Rae, C.M., Garzoli, S.L., Gordon, A.L., 1996. The eddy field of the southeast Atlantic Ocean: a statistical census from the Benguela Sources and Transports Project. J. Geophys. Res. 101 (C5), 11949–11964.

Enderton, D., Marshall, J., 2009. Controls on the total dynamical heat transport of the atmosphere and oceans. J. Atmos. Sci. 66, 1593–1611.

Fasullo, J.T., Trenberth, K.E., 2008. The annual cycle of the energy budget: part 2. Meridional structures and poleward transports. J. Clim. 21, 2313–2325.

Fennig, K., Andersson, A., Bakan, S., Klepp, C., Schroeder, M., 2012. Hamburg Ocean Atmosphere Parameters and Fluxes from Satellite Data—HOAPS 3.2—Monthly Means/6-Hourly Composites. Satellite Application Facility on Climate Monitoring. http://dx.doi.org/10.5676/EUM_SAF_CM/HOAPS/V001.

Festa, J.F., Molinari, R.L., 1992. An evaluation of the WOCE volunteer observing ship–XBT network in the Atlantic. J. Atmos. Oceanic Technol. 9, 305–317.

Fillenbaum, E.R., Lee, T.N., Johns, W.E., Zantopp, R.J., 1997. Meridional heat transport at 26.5° N in North Atlantic. J. Phys. Oceanogr. 27, 153–174.

Friedrichs, M.A.M., Hall, M.M., 1993. Deep circulation in the tropical Atlantic. J. Mar. Res. 51, 697–736.

Ganachaud, A., Wunsch, C., 2000. The oceanic meridional overturning circulation, mixing, bottom water formation, and heat transport. Nature 408, 453–457.

Ganachaud, A., Wunsch, C., 2003. Large-scale ocean heat and freshwater transports during the world ocean circulation experiment. J. Clim. 16, 696–705.

Garnier, E., Barnier, B., Siefridt, L., Béranger, K., 2000. Investigating the 15 years air–sea flux climatology from the ECMWF re-analysis project as a surface boundary condition for ocean models. Int. J. Climatol. 20 (14), 1653–1673.

Garzoli, S.L., Baringer, M.O., 2007. Meridional heat transport determined with expendable bathythermographs. Part II: South Atlantic transport. Deep Sea Res. Part I 54, 1402–1420.

Garzoli, S.L., Baringer, M., Dong, S., Perez, R., Yao, Q., 2012. South Atlantic meridional fluxes. Deep Sea Res. Part I 71, 21–32. http://dx.doi.org/10.1016/j.dsr.2012.09.003.

Garzoli, S.L., Matano, R., 2011. The South Atlantic and the Atlantic meridional overturning circulation. Deep Sea Res. Part II 58, 1837–1847.

Gibson, J.K., Kallberg, P., Uppala, S., Noumura, A., Hernandez, A., Serrano, E., 1997. ERA Description. ECMWF Re-Analysis Project Report Series, vol. 1. ECMWF, Reading, UK, 77 pp.

Giese, B.S., Ray, S., 2011. El Niño variability in simple ocean data assimilation (SODA), 1871–2008. J. Geophys. Res. 116, C02024. http://dx.doi.org/10.1029/2010JC006695.

Gille, S.T., 2003. Float observations of the Southern Ocean. Part II: eddy fluxes. J. Phys. Oceanogr. 33, 1182–1196.

Grist, J.P., Josey, S.A., 2003. Inverse analysis adjustment of the SOC air–sea flux climatology using ocean heat transport constraints. J. Clim. 20, 3274–3295.

Haines, K., Valdivieso, M., Zuo, H., Stepanov, V.N., 2012. Transports and budgets in a ¼° global ocean reanalysis 1989–2010. Ocean Sci. 8, 333–344.

Hall, M.M., Bryden, H.L., 1982. Direct estimates and mechanisms of ocean heat transport. Deep Sea Res. 29 (3A), 339–359.

Hansen, J., Sato, M., Kharecha, P., 2011. Earth's energy imbalance and implications. Atmos. Chem. Phys. 11, 13421–13449. http://dx.doi.org/10.5194/acp-11-13421-2011.

Hatzianastassiou, N., Matsoukas, C., Hatzidimitriou, D., Pavlakis, C., Drakakis, M., Vardavas, I., 2004. Ten year radiation budget of the Earth: 1984–93. Int. J. Climatol. 24 (14), 1785. http://dx.doi.org/10.1002/joc.1110.

Heimbach, P., Wunsch, C., Ponte, R.M., Forget, G., Hill, C., Utke, J., 2011. Timescales and regions of the sensitivity of the Atlantic meridional volume and heat transport: toward observing system design. Deep Sea Res. Part II 58, 1858–1879.

Hernández-Guerra, A., Joyce, T.M., Fraile-Nuez, E., Vélez Belchí, P., 2009. Using Argo data to investigate the meridional overturning circulation in the North Atlantic. Deep Sea Res. Part I 57, 29–36.

Heywood, K.J., Stevens, D.P., 2007. Meridional heat transport across the Antarctic Circumpolar Current by the Antarctic Bottom Water overturning cell. Geophys. Res. Lett. 34, L11610. http://dx.doi.org/10.1029/2007GL030130.

Hobbs, W., Willis, J.K., 2012. Estimates of North Atlantic heat transport from satellite and drifter data. J. Geophys. Res. 17 (C01008). http://dx.doi.org/10.1029/2011JC007039.

Hogg, A. McC, Meredith, M.P., Blundell, J.R., Wilson, C., 2008. Eddy heat flux in the Southern Ocean: response to variable wind forcing. J. Clim. 21 (4), 608–620.

Holfort, J., Siedler, G., 2001. The Meridional Oceanic transports of heat and nutrients in the South Atlantic. J. Phys. Oceanogr. 31, 5–29.

House, F.B., Gruber, A., Hunt, G.E., Mecherikunnel, A.T., 1986. History of satellite missions and measurements of the earth radiation budget (1957-1984). Rev. Geophys. 24, 357–377. http://dx.doi.org/10.1029/RG024i002p00357.

Hunt, G.E., Kandel, R., Mecherikunnel, A.T., 1986. A history of presatellite investigations of the earth's radiation budget. Rev. Geophys. 24, 351–356. http://dx.doi.org/10.1029/RG024i002p00351.

Ichikawa, H., Beardsley, R.C., 1993. Temporal and spatial variability of volume transport of the Kuroshio in the East China Sea. Deep Sea Res. 40, 583–605.

Imawaki, S., Uchida, H., Ichikawa, H., Fukasawa, M., Umatani, S., the ASUKA Group, 2001. Satellite altimeter monitoring the Kuroshio transport south of Japan. Geophys. Res. Lett. 24 (1), 17–20.

Jayne, S.R., Marotzke, J., 2001. The dynamics of ocean heat transport variability. Rev. Geophys. 39, 385–412.

Jayne, S.R., Hogg, N.G., Waterman, S.N., Rainville, L., Donohue, K.A., Watts, D.R., Tracey, K.L., McClean, J.L., Maltrud, M.E., Qiu, B., Chen, S., Hacker, P., 2009. The Kuroshio Extension and its recirculation gyres. Deep Sea Res. Part I 56, 2088–2099.

Johns, W.E., Baringer, M.O., Beal, L.M., Cunningham, S.A., Kanzow, T., Bryden, H.L., Hirschi, J.J.M., Marotzke, J., Meinen, C.S., Shaw, B., Curry, R., 2011. Continuous array-based estimates of Atlantic Ocean heat transport at 26.5°N. J. Clim. 24, 2429–2449.

Johnson, G.C., Sloyan, B.M., Kessler, W.S., McTaggart, K.E., 2002. Direct measurements of upper ocean currents and water properties across the tropical Pacific during the 1990s. Prog. Oceanogr. 52, 31–61.

Josey, S., Kent, E.C., Taylor, P.K., 1998. The Southampton Oceanography Centre (SOC) Ocean-Atmosphere, Heat, Momentum and Freshwater Flux Atlas. Report 6. Southampton Oceanography Centre, UK, 30 pp.

Jung, G.H., 1952. Note on the meridional transport of energy by the ocean. J. Mar. Res. 11, 139–146.

Kalnay, E., Kanamitsu, M., Kistler, R., Collins, W., Deaven, D., Gandin, L., Iredell, M., Saha, S., White, G., Woollen, J., Zhu, Y., Leetmaa, A., Reynolds, R., Chelliah, M., Ebisuzaki, W., Higgins, W., Janowiak, J., Mo, K.C., Ropelewski, C., Wang, J., Jenne, R., Joseph, D., 1996. The NCEP/NCAR 40-year reanalysis project. Bull. Am. Meteorol. Soc. 77, 437–470. http://dx.doi.org/10.1175/1520-0477, 077<0437:TNYRP>2.0.CO;2.

Kanzow, T., Cunningham, S.A., Johns, W.E., Hirschi, J.J.-M., Marotzke, J., Baringer, M.O., Meinen, C.S., Chidichimo, M.P., Atkinson, C., Beal, L.M., Bryden, H.L., Collins, J., 2010. Seasonal variability of the Atlantic meridional overturning circulation at 26.5°N. J. Clim. 23. http://dx.doi.org/10.1175/2010JCLI3389.1171.

Kanzow, T., Cunningham, S.A., Rayner, D., Hirschi, J.J.-M., Johns, W.E., Baringer, M.O., Bryden, H.L., Beal, L.M., Meinen, C.S., Marotzke, J., 2007. Observed flow compensation associated with the meridional overturning circulation near 26.5°N in the Atlantic. Science 317, 938–941. http://dx.doi.org/10.1126/science.1141293.

Kanzow, T., Hirschi, J.J.-M., Meinen, C.S., Rayner, D., Cunningham, S.A., Marotzke, J., Johns, W.E., Bryden, H.L., Beal, L.M., Baringer, M.O., 2008. A prototype system of observing the Atlantic Meridional Overturning Circulation: scientific basis, measurement and risk mitigation strategies, and first results. J. Oper. Oceanogr. 1, 19–28.

Klein, B., Molinari, R.L., Müller, T.J., Siedler, G., 1995. A transatlantic section at 24.5°N: meridional volume and heat fluxes. J. Mar. Res. 53, 929–957.

Koltermann, K.P., Sokov, A.V., Tereschenkov, V.P., Dobroliubov, S.A., Lorbacher, K., Sy, A., 1999. Decadal changes in the thermohaline circulation of the North Atlantic. Deep Sea Res. Part II 46, 109–138.

Large, W.G., Danabasoglu, G., Doney, S.C., McWilliams, J.C., 1997. Sensitivity to surface forcing and boundary layer mixing in a global ocean model: annual-mean climatology. J. Phys. Oceanogr. 27, 2418–2447.

Large, W.G., Yeager, S.G., 2009. The global climatology of an interannually varying air–sea flux data set. Clim. Dyn. 33, 341–364.

Lavín, A., Bryden, H.L., Parrilla, G., 1998. Meridional transport and heat flux variations in the subtropical North Atlantic. Glob. Atmos. Ocean Syst. 6, 269–293.

Lavín, A., Bryden, H.L., Parrilla, G., 2003. Mechanisms of heat, freshwater, oxygen and nutrient transports and budgets at 24.5°N in the subtropical North Atlantic. Deep Sea Res. Part I 50 (9), 1099–1128.

Lawson, C.L., Hanson, D.J., 1974. Solving Least Squares Problems. Prentice-Hall, Englewood Cliffs, NJ.

Lee III, R.B., Gibson, M.A., Wilson, R.S., Thomas, S., 1995. Long-term total solar irradiance variability during sunspot cycle 22. J. Geophys. Res. 100 (A2), 1667–1675.

Liu, H., Liu, X., Zhang, M., Lin, W., 2011a. A critical evaluation of the upper ocean heat budget in the Climate Forecast System Reanalysis data for the south central equatorial Pacific. Environ. Res. Lett. 6, 034022. http://dx.doi.org/10.1088/1748-9326/6/3/034022.

Liu, J., Xiao, T., Chen, L., 2011b. Intercomparisons of air–sea heat fluxes over the Southern Ocean. J. Clim. 24, 1198–1211.

Loeb, N.G., Kato, S., Wielicki, B.A., 2002. Defining top-of-the-atmosphere flux reference level for earth radiation budget studies. J. Clim. 15, 3301–3309.

London, J., 1957. A study of the atmospheric heat balance. New York, USA. Final report, contract USAF8S1911221165, New York University.

Longworth, H.R., Bryden, H.L., Baringer, M.O., 2011. Historical variability in Atlantic meridional baroclinic transport at 26.5°N from boundary dynamic height observations. Deep Sea Res. Part II 58 (17–18), 1754–1767. http://dx.doi.org/10.1016/j.dsr2.2010.10.057.

Lumpkin, R., Speer, K., 2003. Large-scale vertical and horizontal circulation in the North Atlantic Ocean. J. Phys. Oceanogr. 33, 1902–1920.

Lumpkin, R., Speer, K., 2007. Global Ocean meridional overturning. J. Phys. Oceanogr. 37, 2550–2562.

Lumpkin, R., Speer, K.G., Koltermann, K.P., 2008. Transport across 48°N in the Atlantic Ocean. J. Phys. Oceanogr. 38, 733–752.

Macdonald, A.M., 1993. Property fluxes at 30°S and their implications for the Pacific–Indian throughflow and the global heat budget. J. Geophys. Res. 98 (C4), 6851–6868.

Macdonald, A.M., 1998. The global ocean circulation: a hydrographic estimate and regional analysis. Prog. Oceanogr. 41, 281–382.

Macdonald, A.M., Mecking, S., Robbins, P.E., Toole, J.M., Johnson, G.C., Talley, L., Cook, M., Wijffels, S.E., 2009. The WOCE-era 3-D Pacific Ocean circulation and heat budget. Prog. Oceanogr. 82, 281–325.

Marin, F., 1998. Heat flux estimates across A6 and A7 WOCE sections. International WOCE Newsletter 31, 28–31.

McCarthy, G., Frajka-Williams, E., Johns, W.E., Baringer, M.O., Meinen, C.S., Bryden, H.L., Rayner, D., Duchez, A., Roberts, C., Cunningham, S.A., 2012. Observed interannual variability of the Atlantic meridional overturning circulation at 26.5°N. Geophys. Res. Lett. 39, L19609. http://dx.doi.org/10.1029/2012GL052933.

McDonagh, E.L., King, B.A., 2005. Oceanic fluxes in the South Atlantic. J. Phys. Oceanogr. 35, 109–122.

McDonagh, E.L., McLeod, P., King, B.A., Bryden, H.L., Valdés, V.T., 2010. Circulation, heat, and freshwater transport at 36°N in the Atlantic. J. Phys. Oceanogr. 40, 2661–2678.

Meinen, C.S., Baringer, M.O., Garcia, R.F., 2010. Florida Current transport variability: an analysis of annual and longer-periods. Deep Sea Res. Part I 57 (7), 835–846. http://dx.doi.org/10.1016/j.dsr.2010.04.001.

Meinen, C.S., Baringer, M.O., Garzoli, S.L., 2006. Variability in deep western boundary current transports: preliminary results from 26.5°N in the Atlantic. Geophys. Res. Lett. 33, L17610. http://dx.doi.org/10.1029/2006GL026965.

Meredith, M.P., Naveira Garabato, A.C., Hogg, A. McC, Farneti, R., 2012. Sensitivity of the overturning circulation in the Southern Ocean to decadal changes in wind forcing. J. Clim. 25, 99–110.

Molinari, R.L., Johns, E., Festa, J.F., 1990. The annual cycle of meridional heat flux in the Atlantic Ocean at 26.5°N. J. Phys. Oceanogr. 20, 476–482.

Moore, G.W.K., Refrew, I.A., 2002. An assessment of the surface turbulent heat fluxes from the NCEP–NCAR reanalysis over the Western Boundary currents. J. Clim. 15, 2020–2037.

Msadek, R., 2011. Comparing the meridional heat transport at 26.5°N and its relationship with the MOC in two CMIP5. WCRP Open Science Conference, Denver, USA, October 24–28, 2011.

Onogi, K., Tsutsui, J., Koide, H., Sakamoto, M., Kobayashi, S., Hatsushika, H., Matsumoto, T., Yamazaki, N., Kamahori, H., Takahashi, K., Kadokura, S., Wada, K., Kato, K., Oyama, R., Ose, T., Mannoji, N., Taira, R., 2007. The JRA-25 reanalysis. J. Meteorol. Soc. Jpn. 85, 369–432.

Pandey, V.K., Pandey, A.C., 2006. Heat transport through Indonesian throughflow. J. Indian Geophys. Union 10 (4), 273–277.

Rayner, D., Hirschi, J.J.-M., Kanzow, T., Johns, W.E., Cuningham, S.A., Wright, P.G., Frajka-Williams, E., Bryden, H.L., Meinen, C.S., Baringer, M.O., Marotzke, J., Beal, L.M., 2011. Monitoring the Atlantic meridional overturning circulation. Deep Sea Res. Part II 58, 1744–1753. http://dx.doi.org/10.1016/j.dsr2.2010.10.056.

Reid, J.L., 1994. On the total geostrophic circulation of the North Atlantic Ocean: flow patterns, tracers, and transports. Prog. Oceanogr. 33, 1–92.

Rintoul, S., 1991. South Atlantic interbasin exchange. J. Geophys. Res. 96, 2675–2692.

Roemmich, D., Gilson, J., 2011. Ocean circulation and the mass and heat budgets of large ocean regions. First XBT Science Workshop July 7-8, 2011, Melbourne, Australia.

Roemmich, D., Gilson, J., Cornuelle, B., Weller, R., 2001. Mean and time-varying transport of heat at the tropical/subtropical boundary of the North Pacific Ocean. J. Geophys. Res. 106 (C5), 8957–8970.

Roemmich, D., McCallister, T., 1989. Large scale circulation of the North Pacific Ocean. Prog. Oceanogr. 22, 171–204.

Roemmich, D., Owens, W.B., 2000. The Argo Project: global ocean observations for understanding and prediction of climate variability. Oceanography 13, 45–50.

Roemmich, D., Wunsch, C., 1985. Two transatlantic sections: meridional circulation and heat flux in the subtropical North Atlantic Ocean. J. Phys. Oceanogr. 32, 619–664.

Saha, S., Moorthi, S., Pan, H.-L., Wu, X., Wang, J., Nadiga, S., Tripp, P., Kistler, R., Woollen, J., Behringer, D., Liu, H., Stokes, D., Grumbine, R., Gayno, G., Wang, J., Hou, Y.-T., Chuang, H.-Y., Juang, H.-M.H., Sela, J., Iredell, M., Treadon, R., Kleist, D., Van Delst, P., Keyser, D., Derber, J., Ek, M., Meng, J., Wei, H., Yang, R., Lord, S., Van Den Dool, H., Kumar, A., Wang, W., Long, C., Chelliah, M., Xue, Y., Huang, B., Schemm, K.-K., Ebisuzaki, W., Lin, R., Xie, P., Chen, M., Zhou, S., Higgins, W., Zou, C.Z., Liu, Q., Chen, Y., Han, Y., Cucurull, L., Reynolds, R.W., Rutledge, G., Goldberg, M., 2010. The NCEP Climate Forecast System Reanalysis. Bull. Am. Meteorol. Soc. 91, 1015–1057. http://dx.doi.org/10.1175/2010BAMS3001.1.

Sarojini, B.B., Gregory, J.M., Tailleux, R., Bigg, G., Blaker, A., Cameron, D., Edwards, N., Megann, A., Shaffrey, L., Sinha, B., 2011. High frequency variability of the Atlantic meridional overturning circulation. Ocean Sci. 7, 471–486. http://dx.doi.org/10.5194/os-7-471-2011.

Sato, O.T., Rossby, T., 2000. Seasonal and low-frequency variability of the meridional heat flux at 36°N in the North Atlantic. J. Phys. Oceanogr. 30, 606–621.

Saunders, P.M., King, B.A., 1995. Oceanic fluxes on the WOCE A11 section. J. Phys. Oceanogr. 25, 1942–1958.

Schmittner, A., Latif, M., Schneider, B., 2005. Model projections of the North Atlantic thermohaline circulation for the 21st century assessed by observations. Geophys. Res. Lett. 32. http://dx.doi.org/10.1029/2005GL024368, L23710.

Schott, F.A., Xie, S.-P., McCreary Jr., J.P., 2009. Indian Ocean circulation and climate variability. Rev. Geophys. 47. http://dx.doi.org/10.1029/2007RG000245, RG1002.

Send, U., Lankhorst, M., Kanzow, T., 2011. Observation of decadal change in the Atlantic meridional overturning circulation using 10 years of continuous transport data. Geophys. Res. Lett. 38, L24606. http://dx.doi.org/10.1029/2011GL049801.

Shie, C.-L., Hilburn, K., Chiu, L. S., Adler, R., Lin, I.-I., Nelkin, E., Ardizzone, J., Gao, S., 2012. Goddard Satellite-Based Surface Turbulent Fluxes, Daily Grid, version 3. In: Savtchenko, A. (Ed.), Goddard Earth Science Data and Information Services Center (GES DISC), Greenbelt, MD, USA., Accessed at http://dx.doi.org/10.5067/MEASURES/GSSTF/DATA301.

Siqueira, L., Nobre, P., 2006. Tropical Atlantic sea surface temperature and heat flux simulations in a coupled GCM. Geophys. Res. Lett. 33, L15708. http://dx.doi.org/10.1029/2006GL026528.

Sloyan, B.M., Rintoul, S.R., 2001. The Southern Ocean limb of the global deep overturning circulation. J. Phys. Oceanogr. 31, 143–173.

Smith, S.R., Hughes, P.J., Bourassa, M.A., 2011. A comparison of nine air-sea flux products. Int. J. Climatol. 31, 1002–1027.

Speer, K., Holfort, J., Reynaud, T., Siedler, G., 1996. South Atlantic heat transport at 11°S. In: Wefer, G. et al., (Eds.), The South Atlantic: Present and Past Circulation. Springer-Verlag, Berlin, pp. 105–120.

Sprintall, J., Liu, W.T., 2005. Ekman mass and heat transport in the Indonesian seas. Oceanography 18 (4), 88–97.

Stammer, D., Wunsch, C., Giering, R., Ekert, C., Heimbach, P., Marotzke, J., Adcroft, A., Hill, C., Marshall, J., 2002. The global ocean circulation during 1992–1997, estimated from ocean observations and a general circulation model. J. Geophys. Res. 107 (C9), 3118. http://dx.doi.org/10.1029/2001JC000888.

Stammer, D., Wunsch, C., Giering, R., Ekert, C., Heimbach, P., Marotzke, J., Adcroft, A., Hill, C., Marshall, J., 2003. Volume, heat, and freshwater transports of the global ocean circulation 1993–2000, estimated from a general circulation model constrained by World Ocean Circulation Experiment (WOCE) data. J. Geophys. Res. 108 (C1), 3007. http://dx.doi.org/10.1029/2001JC001115.

Stephenson Jr., G.R., Gille, S.T., Sprintall, J., 2012. Seasonal variability of upper ocean heat content in Drake Passage. J. Geophys. Res. 117, C04019. http://dx.doi.org/10.1029/2011JC007772.

Sultan, E., Mercier, H., Pollard, R.T., 2007. An inverse model of the large scale circulation in the South Indian Ocean. Prog. Phys. Oceanogr. 74, 71–94.

Sun, C., Watts, D.R., 2002. Heat flux carried by the Antarctic Circumpolar Current mean flow. J. Geophys. Res. 107 (C9), 3119. http://dx.doi.org/10.1029/ 2001JC001187.

Sverdrup, H.U., 1957. Oceanography. In: Bartels, J. (Ed.), Handbuch der Physik, 48. Springer-Verlag, Berlin, pp. 608–670.

Swart, S., Speich, S., Ansorge, I.J., Goni, G.J., Gladyshev, S., Lutjeharms, J.R.E., 2008. Transport and variability of the Antarctic Circumpolar Current south of Africa. J. Geophys. Res. 113 (C09014). http://dx.doi.org/10.1029/2007JC004223.

Talley, L.D., 2003. Shallow, intermediate and deep overturning components of the global heat budget. J. Phys. Oceanogr. 33, 530–560.

Thompson, D.W.J., Solomon, S., 2002. Interpretation of recent Southern Hemisphere climate change. Science 296, 895–899.

Tomita, H., Kubota, M., Cronin, M.F., Iwasaki, S., Konda, M., Ichikawa, H., 2010. An assessment of surface heat fluxes from J-OFURO2 at the KEO and JKEO sites. J. Geophys. Res. 115, C03018. http://dx.doi.org/10.1029/2009JC005545.

Trenberth, K.E., Fasullo, J.T., Kiehl, J., 2009. Earth's global energy budget. Bull. Am. Meteorol. Soc. 90 (3), 311–323.

Trenberth, K.E., Fasullo, J.T., Mackard, J., 2011. Atmospheric moisture transports from ocean to land and global energy flows in reanalyses. J. Clim. 24, 4907–4924.

Trenberth, K.E., Smith, L., 2009. The three dimensional structure of the atmospheric energy budget: methodology and evaluation. Clim. Dyn. 32, 1065–1079.

Uehara, H., Kizu, S., Hanawa, K., Yoshikawa, Y., Roemmich, D., 2008. Estimation of heat and freshwater transports in the North Pacific using high-resolution expendable bathythermograph data. J. Geophys. Res. 113, C02014. http://dx.doi.org/10.1029/2007JC00.

Uppala, S.M., Kållberg, P.W., Simmons, A.J., Andrae, U., da Costa Bechtold, V., Fiorino, M., Gibson, J.K., Haseler, J., Hernandez, A., Kelly, G.A., Li, X., Onogi, K., Saarinen, S., Sokka, N., Allan, R.P., Andersson, E., Arpe, K., Balmaseda, M.A., Beljaars, A.C.M., van de Berg, L., Bidlot, J., Bormann, N., Caires, S., Chevallier, F., Dethof, A., Dragosavac, M., Fisher, M., Fuentes, M., Hagemann, S., Holm, E., Hoskins, B.J., Isaksen, L., Janssen, P.A.E.M., Jenne, R., McNally, A.P., Mahfouf, J.-F., Morcrette, J.-J., Rayner, N.A., Saunders, R.W., Simon, P., Sterl, A., Trenberth, K.E., Untch, A., Vasiljevic, D., Viterbo, P., Woollen, J., 2005. The ERA-40 re-analysis. Q. J. R. Meteorol. Soc. 131, 2961–3012.

van Sebille, E., Baringer, M.O., Johns, W.E., Meinen, C.S., Beal, L.M., Femke de Jong, M., van Aken, H.M., 2011. Propagation pathways of classical Labrador Sea Water from its source region to 26°N. J. Geophys. Res. 116, C12027. http://dx.doi.org/10.1029/2011JC007171.

Vranes, K., Gordon, A.L., Ffield, A., 2002. The heat transport of the Indonesian throughflow and implications for the Indian Ocean heat budget. Deep Sea Res. 49, 1391–1410.

Volkov, D.L., Fu, L.-L., Lee, T., 2010. Mechanisms of the meridional heat transport in the Southern Ocean. Ocean Dyn. 60, 791–801.

Wang, J., Carton, J.A., 2002. Seasonal Heat Budgets of the North Pacific and North Atlantic Oceans. J. Phys. Oceanogr. 32, 3474–3489.

Wang, W., Xie, P., Yoo, S.-H., Xue, Y., Kumar, A., Wu, X., 2011. An assessment of the surface climate in the NCEP climate forecast system reanalysis. Clim. Dyn. 37, 1601–1620.

Warren, B.A., 1999. Approximating the energy transport across oceanic sections. J. Geophys. Res. 104, 7915–7979.

Weijer, W., De Ruijter, W.P.M., Sterl, A., Drijfhout, S.S., 2002. Response of the Atlantic overturning circulation to South Atlantic sources of buoyancy. Glob. Planet. Change 34, 293–311.

Wiggins, R.A., 1972. The general linear inverse problem: implication of surface waves and free oscillations for earth structure. Rev. Geophys. Space Phys. 10, 251–283.

Wijffels, S.E., Toole, J.M., Bryden, H.L., Fine, R.A., Jenkins, W.J., Bullister, J.L., 1996. The water masses and circulation at 10°N in the Pacific. Deep Sea Res. 43, 501–544.

Wijffels, S.E., Toole, J.M., Davis, R., 2001. Revisiting the South Pacific subtropical circulation: a synthesis of World Ocean Circulation Experiment observations along 32°S. J. Geophys. Res. 106, 19481–19513.

Willis, J.K., 2010. Can *in situ* floats and satellite altimeters detect long-term changes in Atlantic Ocean overturning? Geophys. Res. Lett. 37, L06602. http://dx.doi.org/10.1029/ 2010GL042372.

Willson, R.C., Hudson, H.S., 1991. The sun's luminosity over a complete lunar cycle. Nature 351, 41–44.

Wunsch, C., 1977. Determining the general circulation of the oceans: a preliminary discussion. Science 196, 871–875.

Wunsch, C., 1996. The Ocean Circulation Inverse Problem. Cambridge University Press, 442 pp.

Wunsch, C., Heimbach, P., 2009. The global zonally integrated ocean circulation, 1992–2006: seasonal and decadal variability. J. Phys. Oceanogr. 39, 351–368.

Wunsch, C.,Heimbach, P., 2013. Dynamically and kinematically consistent global ocean circulation and ice state estimates.

Wüst, G., Defant, A., 1936. Atlas zur Zirculation des Atlantischen Ozeans, VI. Walter de Gruyter and Co., Berlin/Leipzig, Germany, 103 pp.

Yu, L.S., Jin, X., Weller, R.A., 2008. Multidecade Global Flux Datasets from the Objectively Analyzed Air–sea Fluxes (OAFlux) Project: Latent and Sensible Heat Fluxes, Ocean Evaporation, and Related Surface Meteorological Variables. OAFlux Project Technical Report (OA-2008-01), Woods Hole, Woods Hole Oceanographic Institution, USA.

Yu, L.S., Weller, R.A., Sun, B., 2004. Improving latent and sensible heat flux estimates for the Atlantic Ocean (1988–1999) by a synthesis approach. J. Clim. 17, 373–393.

Zheng, Y., Giese, B.S., 2009. Ocean heat transport in simple ocean data assimilation: structure and mechanisms. J. Geophys. Res. 114. http://dx.doi.org/10.1029/2008JC005190.